In situ fluid dynamics and CO_2 injection in porous rocks

Amund Brautaset

Dissertation for the degree philosophiae doctor (PhD)
at the University of Bergen

Bergen, October 2009

Preface

This dissertation is submitted to the Department of Physics and Technology, Faculty of Mathematics and Natural Sciences, University of Bergen in the partial fulfillment of the requirements for the degree philosophiae doctor (PhD) and serves as documentation of my work during my PhD study. This dissertation summarizes experimental work done over the past three years in laboratories at the University of Bergen and at the ConocoPhillips Technology Center in Bartlesville, Oklahoma, USA. The work has been funded by the Norwegian Research Council as part of the project "*Enhanced oil recovery in fractured carbonate reservoirs*".

Table of contents

Summary

Understanding multiphase fluid flow in porous rocks implies knowledge of fundamental properties such as wettability, relative permeability and capillary pressure. These parameters, as well as the extent of fractures and their permeability and interconnection, are vital information needed to predict oil recovery, select production scenario and initiate EOR strategies in the reservoir. In this thesis, wettability, relative permeability and capillary pressure are measured directly from *in situ* saturation and pressure data and the impacts on oil recovery from capillary continuity across fractures have been studied. Finally, injection of CO_2 to enhance oil recovery is investigated at different wettabilities and when varying a wide range of injection scenarios.

Conventionally, relative permeability curves are generated from capillary pressure curves using best-fit analyses of the production data. Experimental methods to measure relative permeability include unsteady-state methods which are based on production data and average pressure drop across entire core samples. They may thus fail to capture capillary end effects and local variations and heterogeneities. The steady-state methods claim to describe dynamic properties but rely on pressure or saturation equilibrium. Alternatively, some steady-state methods are based on simultaneous injection of one wetting and one non-wetting fluid phase but aim to describe the properties of either drainage or imbibition processes.

An alternative, explicit method to calculate relative permeabilities has been reviewed and slightly modified in this thesis, and dynamic capillary pressure curves have been measured at different wettabilities based on *in situ* saturation and phase pressure data collected during continuous flooding. Both methods utilize dynamic measurements to describe the properties of relative permeability and capillary pressure as opposed to most conventional methods. The relative permeability curves showed consistency with wettability, and a good match with conventional curves at strongly water-wet conditions was obtained. The capillary pressure curves corroborated data obtained from centrifuge experiments at strongly water-wet, less water-wet and near neutral-wet conditions. In addition, the proposed methods for obtaining both relative permeability and capillary pressure curves are time-saving, and *in situ* data increased the accuracy and confidence of the input to numerical simulators used to predict reservoir fluid flow.

A drawback with the conventional Amott-Harvey Index of wettability measurement method is the time consumed from obtaining spontaneous imbibition data. The possibility to capture local heterogeneities is also limited in this method, as the data collected from imbibition and subsequent water- or oilfloods are average measures obtained from whole core samples. In this work, local wettability indices are measured during continuous flooding from *in situ* saturation and local pressure data by identifying the separate contributions to oil recovery from spontaneous imbibition and viscous displacement. The obtained wettability indices demonstrate an excellent match with the conventional data.

Previous work has shown that wetting phase bridges across an open fracture establish capillary continuity between two mixed-wet matrix blocks and increase oil recovery exceeding the end-point for spontaneous imbibition. However, the wetting phase produced from the inlet matrix block during drainage of strongly wetted systems forms

a film on the outlet end and fails to establish capillary continuity across the fracture. In this work, capillary continuity in strongly wetted systems has been established during drainage processes by packing the separating fracture with micro-particles. Capillary continuity was determined by monitoring the volume accumulated by the capillary end effect during continuous injection of the non-wetting phase.

The demand for enhanced oil recovery in mature oil fields combined with carbon neutral solutions and high quality *in situ* data is increasing. Several projects have been initiated worldwide to capture CO_2 from fossil fuel-fired power plants and other industrial processes, and CO_2 is thus becoming more available for EOR projects. In order to further increase the understanding of multiphase dynamic fluid flow in porous media, MRI was used to monitor *in situ* saturation development during injection of liquid or supercritical CO_2 at different wettabilities and at miscible conditions. A series of experiments was initiated to study oil recovery potential from injection of compressed CO_2 at secondary and tertiary conditions, monitor *in situ* fluid flow and investigate oil recovery mechanisms in low-permeable outcrop chalk. Qualitative analysis of the MRI images indicated oil swelling at the front as the CO_2 propagated through the cores, and enhanced oil recovery ranging from 9.4 %PV to 67 %PV was determined from material balance calculations. During tertiary injection of liquid CO_2 in a fractured core sample, MRI images suggested that the oil in the middle and outlet end of the core was bypassed due to high fracture permeability.

The results obtained from the various experiments emphasize the importance of using high spatial resolution saturation imaging, providing increased understanding of multiphase *in situ* fluid flow in porous media, assisting in predicting recovery mechanisms and improving input data used in numerical simulators.

Acknowledgements

I wish to acknowledge the Norwegian Research Council for providing financial support and research funding for this thesis, which is part of an ongoing research project entitled "*Enhanced oil recovery in fractured carbonate reservoirs*".

First and foremost, I want to thank my supervisor Arne Graue at the Department of Physics and Technology at the University of Bergen for his excellent guidance, his ability to motivate his students and for providing ideal working conditions.

I want to thank the mechanical workshop at the Department of Physics and Technology, and especially head engineer Kåre Slettebakken for his remarkable ability to provide solutions to mechanical problems, for his excellent craftsmanship and for showing up on a Saturday to help me out in the workshop. Without the assistance from him and his crew, this thesis would not exist.

I thank David Zornes and Jim Johnson for inviting students to the ConocoPhillips Technology Center and giving us the opportunity to do research in their labs. Special thanks to Mr. Jim Stevens, the always helpful and highly skilled lab technician for assisting me with my experiments. Many thanks to James Howard and Bernie Baldwin for their professional expertise and for helping me running the MRI.

I will always remember my fellow students at the University of Bergen; Martin Fernø, Geir Ersland, Åsmund Haugen, Øyvind Bull, Jarle Husebø, Are Martinsen and Bergit Brattekås. We have shared challenging discussions, memorable social events and fruitful co-operations. Thank you.

Finally, I wish to express my gratitude to my most supportive, my best encouragers and my biggest motivators; my darling wife Synneva Byrkjeland Grytås and my son Johan Grytås Brautaset.

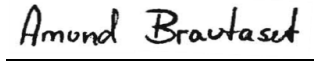

Amund Brautaset

List of publications

Paper 1

Brautaset, A., Ersland, G., Graue, A.: "*In situ Phase Pressures and Fluid Saturation Dynamics Measured in Waterfloods at Various Wettability Conditions*", proceedings at the *2008 SPE Improved Oil Recovery Symposium* held in Tulsa, OK, USA, 19–23 April 2008. Accepted for publication in SPE Reservoir Evaluation and Engineering.

Paper 2

Brautaset, A., Ersland, G., Graue, A.: "*Determining Wettability from In situ Pressure and Saturation Measurements*", submitted to Journal of Petroleum Science and Engineering.

Paper 3

Brautaset, A., Brattekås, B., Haugen, Å., Graue, A.: "*Direct calculation of relative permeabilities from* in situ *phase pressures and fluid saturations*", submitted to Transport in Porous Media.

Paper 4

Brautaset, A., Martinsen, A. S., Graue, A.: "*EOR in Fractured Reservoirs - Capillary Continuity by Fracture Particle Filling*", submitted to Journal of Petroleum Science and Engineering.

Paper 5

Brautaset, A., Ersland, G., Graue, A., Stevens, J. and Howard, J.: "*Using MRI to Study In situ Oil Recovery During CO_2 Injection in Carbonates*", reviewed proceedings at the *SCA International Symposium and Wettability Conference* held in Abu Dhabi, UAE, 26 Nov-02 Dec 2008. Submitted to Journal of Petroleum Science and Engineering.

Paper 6

Brautaset, A., Haugen, Å., Graue, A.: "*Experimental Study of Enhanced Oil Recovery by CO_2 Injection at Various Wettabilities*", submitted to SPE Reservoir Evaluation and Engineering.

Introduction

The concept of improved or enhanced oil recovery has emerged as the global need for supply of oil has increased, and is subject to large investments within all major oil companies. Improved oil recovery strategies include studies of multiphase fluid flow mechanisms, reservoir description and modeling, development of smarter drilling techniques and injection of various types of liquids containing polymers, surfactants, enzymes and foam, gas injection and WAG. As the technology and the tools for modeling and simulating the multiphase fluid flow in the reservoirs are rapidly developing, the need for high quality and preferably *in situ* input data is increasing. The results in this thesis include thorough analyses of the data from various flooding experiments with respect to the *in situ* two and three phase fluid dynamics.

Chapter 1. In situ *fluid dynamics*

Some of the important quantities of reservoir physics and their recent improvements are reviewed in this chapter, including capillary pressure and relative permeability measurements, the notion of dynamic capillary pressure, methods for measuring wettability and its effects on capillary pressure and relative permeability. In addition, theory on three phase fluid dynamics, EOR potential and recovery mechanisms during CO_2 injection are briefly reviewed.

1.1 Two phase *in situ* relative permeability

As two or more immiscible fluids are present in a porous medium, the effective permeability of each fluid phase is reduced due to friction between the phases and less available pore space to each of the fluid phases. Since the friction between the fluid phases remains constant, the effective permeability to each phase only depends on the amount of each phase present at a given time. The relative permeability to a given fluid phase, defined as the effective permeability of that phase divided by the absolute permeability of the porous medium, thus becomes a function of saturation. Accurate relative permeability curves are a powerful tool to reservoir engineers to describe the fluid phase behavior during oil production, but obtaining relative permeability measurements from lab experiments that are valid and field representative often proves difficult. Most conventional methods (Corey, 1954, Johnson *et al.*, 1959, Sigmund and McCaffery, 1979, Heaviside *et al.*, 1983, Chierici, 1984, Lomeland *et al.*, 2005) use inlet pressure and average saturations from the production data to calculate relative permeability, but these methods are coarse approximations which may fail to capture end effects and the local variations or heterogeneities inside the core samples.

With the development of *in situ* saturation measurement techniques such as Nuclear Tracer Imaging (NTI), X-ray Computed Tomography (CT) and Magnetic Resonance Imaging (MRI), the ability to study local saturation variations within core samples has become available.

Using the NTI method to obtain local *in situ* saturation data and a core holder with embedded pressure taps to measure *in situ* pressure data, Kolltveit *et al*. calculated water-oil relative permeabilities from drainage experiments (Kolltveit *et al.*, 1990). During continuous flooding, the *in situ* pressure and saturation measurements provided satisfactory relative permeability curves. However, with some degree of uncertainties in both the pressure and saturation measurement techniques, several approximations and adjustments were necessary.

A method for direct calculations of water-air and water-oil relative permeabilities during spontaneous imbibition experiments was presented by Schembre and Kovscek in 2001, using CT to measure *in situ* saturation profiles during imbibition and accounting for capillary forces (Schembre and Kovscek, 2001). The method is based on accurate saturation measurements, and dynamic relative permeability and capillary pressure are calculated directly from the measured data. The pressure gradients used in the calculations, however, are calculated using the Leverett function and not measured during the experiments. The reported relative permeability curves are thus a product of constructed or simulated pressure data.

Measuring individual phase pressures by using pressure taps and semi-permeable discs with selected wetting preference, Lackner and Torsæter calculated dynamic capillary pressure and simulated relative permeabilities during imbibition and drainage experiments (Lackner and Torsæter, 2005). The saturation calculations were based on material balance measurements and without the use of any *in situ* imaging techniques. The observed differences between the dynamically measured and conventional static capillary pressure and relative permeability curves are explained by possible end effects during static measurements, the low capillary pressures reached during the dynamic method and the improved pressure measurement techniques presented in the paper.

A number of similar methods for relative permeability and capillary pressure measurements have been proposed recent years, but literature covering the combination of *in situ* 3D saturation imaging and local phase pressure measurements during continuous flooding is limited.

1.2 Dynamic capillary pressure and relative permeability

The notion of capillary pressure in a porous medium is based on the pressure difference between two immiscible fluids and the curvature of the interface at static conditions, given by the Laplace law:

$$P_c = \Delta P = P_o - P_w = \sigma_{ow}\left(\frac{1}{R_1} + \frac{1}{R_2}\right) \quad (1)$$

where σ_{ow} is the interfacial tension and R_1 and R_2 are the principal radii of the interface curvature. In a capillary tube, where $R_1 = R_2 = r_c$, the capillary pressure can be expressed as:

$$P_c = \sigma_{ow}\left(\frac{1}{R_1} + \frac{1}{R_2}\right) = \frac{2\sigma_{ow} \cdot cos\,\theta_c}{r_c} \quad (2)$$

where θ_c is the contact angle between the meniscus and the solid surface and r_c is the radius of the capillary pipe. Assuming that a non-wetting phase displaces a wetting phase and that a porous medium can be seen as a set of capillary tubes, for a given capillary pressure level, the menisci will be located at the entry of capillary tubes with a radius equal to $\frac{2\sigma_{ow} \cdot cos\ \theta_c}{P_o - P_w}$. The set of accessible tubes is thus related to a given saturation. The notion of static capillary pressure has conventionally been used to interpret two-phase fluid flow in porous media and to describe the dynamic capillary pressure, although the Laplace law is valid only under static conditions. It has been debated whether the conventional notion of capillary pressure, which is based on static or equilibrium conditions, in fact fully describes the dynamic properties of capillary pressure (Kalaydjian, 1992a, Hassanizadeh *et al.*, 2002, Helmig *et al.*, 2007).

During conventional capillary pressure measurements, average core saturation and inlet pressure is measured at different saturation equilibria. The conventional methods include the mercury injection method, the porous plate method and the centrifuge method (Anderson, 1987a). Other methods for measuring capillary pressure include the direct measurement of saturation method (DMS), the desorption of water vapor method and the semi-dynamic method. Only the direct measurement of saturation method involves *in situ* saturation measurements.

During the mercury injection method, liquid mercury is injected into a core sample which has been extracted, dried and evacuated. By stepwise increasing the injection pressure, the amount of mercury entering the sample is measured and converted to non-wetting phase saturation. The pressure of the gas phase (mercury vapor) is very small, and thus the absolute pressure of the liquid mercury is the capillary pressure. A typical experimental setup of the mercury injection method is illustrated in Figure 1.

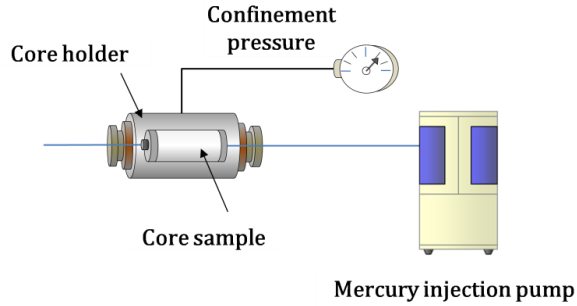

Figure 1: Schematic showing a typical setup for measuring capillary pressure using the mercury injection method. Liquid mercury is injected by stepwise pressure increase, and the amount of injected mercury determines the saturation at each pressure step.

The porous plate method makes use of semi-permeable membranes, which are made of porcelain, cellulose or fused glass with small uniform pores. When saturated with the wetting phase, the membranes exhibit high threshold pressures to a non-wetting phase. The porous plate is stacked with a core sample saturated with the wetting phase as shown in Figure 2. A non-wetting phase is injected by stepwise pressure increase and the wetting phase is produced through the porous plate. By measuring the production at each pressure step, the capillary pressure curve may be calculated.

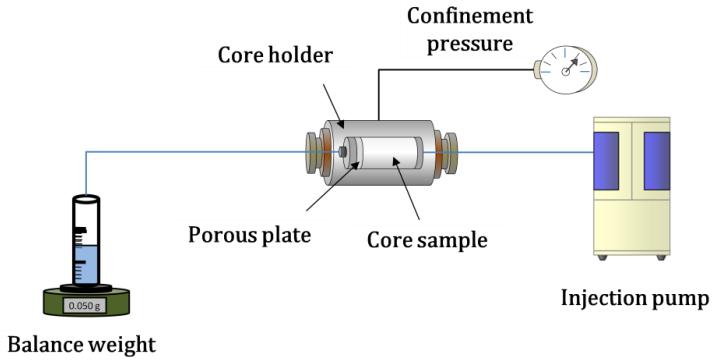

Figure 2: Schematic showing a typical setup for measuring capillary pressure using the porous plate method. A non-wetting phase is injected by stepwise pressure increase from the right, and the wetting phase is produced through a porous plate at the left.

Measuring capillary pressure using the centrifuge method employs a core sample mounted in a core holder and placed in a centrifuge as indicated in Figure 3. By rotating the centrifuge at stepwise increasing speeds, centrifugal force is applied to the fluids saturating the core, and a pressure gradient is generated in each fluid phase according to the density difference. As the first phase is produced at the outlet end, the second phase enters the core at the inlet end. By measuring the cumulative production at equilibrium obtained at each rotational speed, fluid saturations and capillary pressures may be calculated.

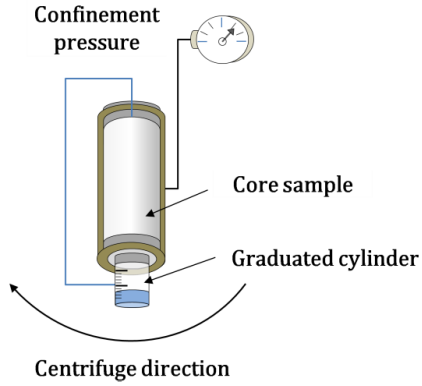

Figure 3: Schematic showing a typical setup for measuring capillary pressure using the centrifuge method. A non-wetting phase is injected at the inlet and the wetting phase is produced at the outlet to reach equilibrium at each rotational speed of the centrifuge.

The direct measurement of saturation method is not recognized as a conventional capillary pressure measurement method. However, it involves measuring *in situ* saturation distributions using MRI or NTI in a centrifuge system similar to the centrifuge method, allowing the effects of local heterogeneities and capillary end effects to be identified. The saturation measurements from all of the four techniques described above are collected at equilibrium at certain injection pressures and they are thus characterized as static or steady-state capillary pressures.

Several attempts have been made to develop dynamic terms by defining dynamic contact angles (Ngan and Dussan, 1982, Calvo *et al.*, 1991, Li and Slattery, 1991). De Gennes proposed an expression of a dynamic capillary pressure for an imbibition process in a homogeneous water-wet porous medium, relating the dynamic capillary pressure to the capillary number N_c and the tortuosity factor τ (de Gennes, 1988):

$$P_{cd} \sim \frac{\sigma_{ow}}{r_t} (N_c)^{2/3} \cdot \tau^{5/3} \quad (3)$$

where r_t is the pore throat radius, N_c is the capillary number and τ is the tortuosity factor. The structure of the porous medium thus has to be taken into account, requiring thin section or similar analysis of the porous medium. A method for measuring unsteady-state or *dynamic* capillary pressure was presented by Kalaydjian in 1992. The method was based on local pressure measurements using embedded pressure taps with semi-permeable discs and local *in situ* saturation measurements using ultrasonic transducers. The technique allows continuous recording of phase pressure and local saturation data during flooding, and a relationship between the dynamic and the conventional static capillary pressure was proposed:

$$P_{c\ dyn} = P_{c\ stat} + \lambda \frac{\partial(\phi s_o)}{\partial t} \quad (4)$$

where λ is a dynamic coefficient and $\frac{\partial(\phi s_o)}{\partial t}$ is the rate of change of the saturation (Kalaydjian, 1992b). The second term on the right-hand side is of dynamic origin and vanishes as the rate tends to zero. It has been shown that dynamic capillary pressure may differ significantly from static capillary pressure due to the influence of the capillary number and fluid velocity on the dynamic capillary pressure (Honarpour *et al.*, 1995). Advantages and disadvantages exist for both static and dynamic measurement techniques, and comparisons between the two are not straight forward due to the different regimes studied in the different measurement techniques. It has been shown that the dynamic capillary pressure is lower than the static capillary pressure during imbibition and higher during drainage processes, and that the dynamic capillary pressure may provide a better representation of a flowing or production scenario than the static capillary pressure (Hassanizadeh *et al.*, 2002).

1.3 Wettability and its effects on P_c and k_r

Wettability can be defined as the ability a rock surface has to retain contact with one fluid phase when two or more immiscible fluids are present. The wettability of a reservoir rock may range from strongly water-wet to intermediate-wet to strongly oil-wet, and is considered an important factor controlling the distribution and fluid flow mechanisms in the reservoir. In a strongly water-wet reservoir rock, water is coating the rock surface, while the oil is located in the center of the pores. Similarly, the oil phase coats the pore surface in an oil-wet reservoir and the water occupies the center of the pores. A fractional-wet system describes a core surface where oil-wet and water-wet areas are randomly distributed in the system regardless of pore size. In mixed-wet systems, oil is coating the surfaces of the larger pores and water is coating the surfaces in the smaller pores or vice versa. Such systems are called mixed-wet large and mixed-wet small, respectively.

The three conventional methods for measuring the wettability of a surface in the laboratory include the contact angle measurement, the Amott-Harvey test (Amott, 1959) and the U.S. Bureau of Mines (USBM) method (Anderson, 1986). Other methods, such as NMR relaxation and resistivity logging, may assist in reservoir wettability determination, given their ability to indicate the wettability *in situ*. Several other methods have been proposed as measures of wettability, including imbibition rates, microscope examination, flotation, the glass slide method, relative permeability curves, the capillarimetric method, displacement capillary pressure, reservoir logs and dye adsorption (Anderson, 1986).

The contact angle method measures the wettability of a specific surface, while the Amott and USBM methods measure the average wettability of a core sample. The contact angle in a water/oil/surface system defines the wettability of that specific surface (Figure 4), and is related to the interfacial tensions (IFTs) in the system by Young's equation:

$$\sigma_{ow} \cdot \cos\theta_c = \sigma_{os} - \sigma_{ws} \tag{5}$$

where σ_{ow} is the IFT between oil and water, θ_c is the contact angle measured through the water, σ_{os} is the IFT between oil and the surface and σ_{ws} is the IFT between water and the surface. When the contact angle is small (less than 60°), the surface is defined as water-wet (Figure 4, below left), and when the contact angle is large (more than 120°), the surface is oil-wet (Figure 4, below right). Contact angles between 60° and 120° define intermediately wetted surfaces (Anderson, 1986).

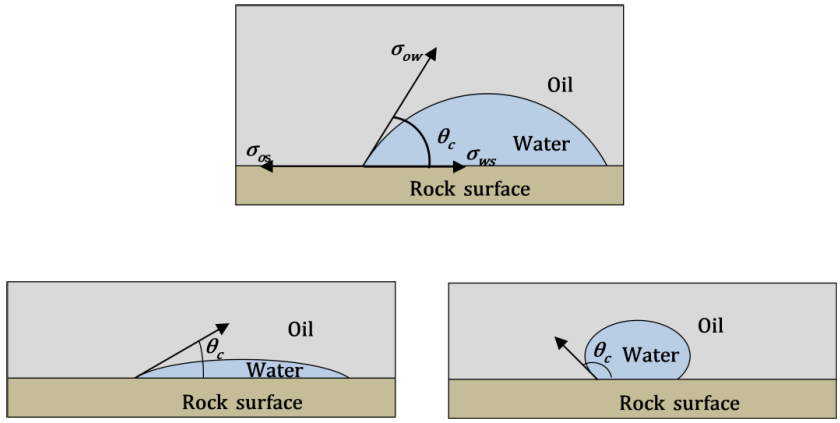

Figure 4: A typical oil-water-rock surface system (top). The relationship between the contact angle and the oil/water, oil/surface and water/surface IFTs are given by the Young equation. A water-wet system (below, left) is characterized by a small contact angle and an oil-wet system (below, right) by a large contact angle.

The Amott-Harvey Index is a volumetric, average measure of wettability, ranging from -1 for oil-wet conditions to +1 for water-wet conditions. A core sample at irreducible water saturation (S_{wi}) is put in an imbibition cell filled with water as shown in Figure 5 (left), and the expelled oil is collected at the top of the graduated cylinder until the end-point for spontaneous imbibition (S_a in Figure 5, right) is reached. The core is waterflooded to S_{or} to obtain the Amott Index of water (I_w), and the same sequence is

repeated with oil to obtain the Amott Index of oil (I_o). The oil index is then subtracted from the water index to obtain the Amott Index of wettability:

$$I_{Amott} = I_w - I_o = \left(\frac{V_{si}}{V_{si}+V_f}\right)_w - \left(\frac{V_{si}}{V_{si}+V_f}\right)_o \quad (6)$$

where v_{si} is the volume produced due to spontaneous imbibition and v_f is the volume produced from forced injection of water (w) or oil (o).

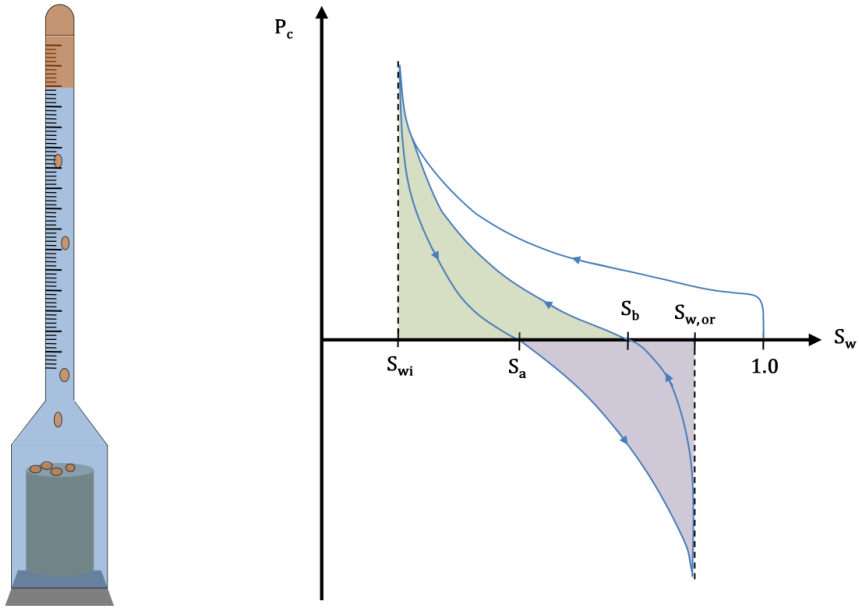

Figure 5: A graduated imbibition cell (left) is used to measure the volume of oil or water produced from spontaneous imbibition. The capillary pressure curve is used to calculate the USBM index (right). S_a *and* S_b *indicate the end-point saturations for spontaneous imbibition of water and oil, respectively.*

The USBM test uses the area under the capillary pressure curve as indicated in Figure 5 (right) as a measure of wettability. The USBM Index is calculated as the logarithm of the ratio of the two areas:

$$I_{USBM} = log\left(\frac{\text{area}_1}{\text{area}_2}\right) \quad (7)$$

where area$_1$ and area$_2$ indicate the area under the positive and negative part of the capillary pressure curve according to Figure 5 (right). At intermediate-wet conditions, the Amott test is an inaccurate method for wettability determination due to the limited volume produced from spontaneous imbibition. Determination of wettability using the Amott test is also a time consuming process, relying on weeks or months of spontaneous imbibition measurements. The USBM method, however, is more sensitive near intermediate-wet conditions, and it is a relatively rapid method compared to the Amott method.

A drawback with the USBM method is the lack of ability to distinguish fractional-wet from mixed-wet conditions. A modification of the USBM method was suggested, which allows simultaneous measurement of the Amott and the USBM indices (Sharma and Wunderlich, 1985). The combined USBM/Amott method accounts for the saturation change at zero capillary pressure, which greatly improves the resolution of the USBM method. In addition, the added Amott measurements may assist in indicating whether an intermediate wetted system is fractional-wet or mixed-wet. In general, wettability greatly impacts the capillary pressure, relative permeabilities and end-point saturations both during drainage and imbibition due to different fluid distributions and flow properties. The following sections briefly summarize the impacts from wettability on capillary pressure and relative permeability.

When a system is strongly water-wet or oil-wet, the wetting phase will spontaneously imbibe into the core and displace the non-wetting phase, and the amount and rate of the spontaneous imbibition is a function of wettability, viscosity, IFT, pore structure and initial saturation (Anderson, 1987a). The end-point saturation after spontaneous imbibition (S_a in Figure 5, right) is a measure of the average wettability of the core sample according to the Amott test.

In a strongly water-wet core sample, the end-point saturation for spontaneous imbibition is close to residual oil saturation, and little or no oil is displaced by water during viscous displacement. In an intermediate-wet or oil-wet core sample, the end-point saturation from spontaneous imbibition is close to irreducible water saturation as little or no water is imbibed into the core. All the produced oil is from viscous displacement, and thus the area under the negative part of the capillary pressure curve (in Figure 5, right) is large. The end-point for spontaneous imbibition of oil (S_b in Figure 5, right), is close to residual oil saturation in a water-wet or intermediate-wet system, and close to irreducible water-saturation at oil-wet conditions.

In strongly water-wet systems, the water relative permeability at residual oil saturation is low due to the oil globules in the center of the pores which effectively reduce the flow of water. Oil relative permeability at irreducible water saturation approaches the absolute permeability, as the water is located in the smaller pores and coating the surface of the larger pores where it has little effect on the flow of oil. In contrast, the water relative permeability at residual oil saturation in oil-wet systems is much higher, as the oil phase now coats the surfaces and allows the water to flow in the center of the pores. The crossover saturation, i.e. the saturation of the wetting phase at which the oil and water relative permeabilities are equal, is generally greater than 50 % in strongly water-wet systems and less than 50 % in oil-wet systems.

The effective oil permeability at irreducible water saturation decreases in a uniformly wetted core sample as the wettability is changed from water-wet to oil-wet conditions. In addition, the water relative permeability increases and the oil relative permeability decreases as the core sample becomes more oil-wet. This also seems to be the case for fractionally wetted sand packs as the fraction of oil-wet surfaces increases. In mixed-wet core samples, the larger, oil-filled pores are oil-wet, and the smaller water-filled pores are water-wet. The continuous oil-path in the larger pores changes the relative permeability curves compared to the uniformly or fractionally wetted cores, and allow the mixed-wet system to be waterflooded to a very low residual oil saturation (Anderson, 1987b).

1.4 Capillary continuity over fractures

Two important factors controlling the oil recovery from fractured reservoirs are matrix wettability and fracture aperture, and governing recovery mechanisms include capillary and viscous forces and gravity. The extent of oil recovery from spontaneous imbibition into the matrix is controlled by wettability, and applying a viscous component to the water may or may not be a source of enhanced recovery depending on wettability, fracture permeability and fracture aperture. In a system of high fracture permeability, the injected water will bypass the matrix blocks, and the oil remains trapped in the reservoir. In fractured, oil-wet systems with no capillary continuity between the matrix blocks, a significant amount of oil is trapped in each block during waterflood due to the capillary end effect (Figure 6, left). In a similar system, but with lower fracture permeability or aperture or with capillary continuity between the matrix blocks, the oil recovery may be significantly increased compared to the system with no capillary continuity by producing the volume of oil captured by the capillary end effect (Figure 6, right).

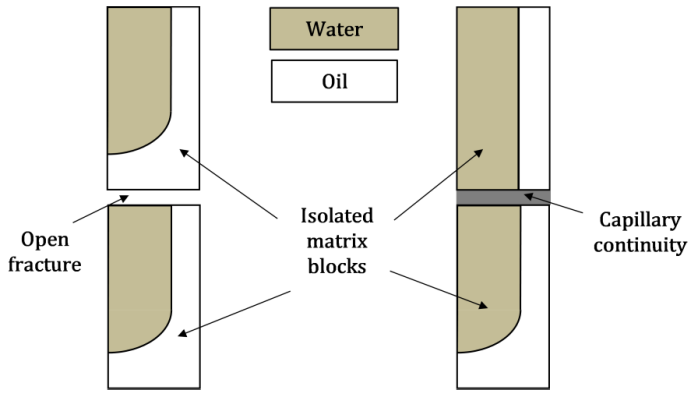

Figure 6: Two vertically stacked, oil-wet matrix blocks with no capillary continuity (left). By establishing capillary continuity, the volume of oil otherwise trapped by the capillary end effect may be produced (right).

Recent studies have proved extra oil recovery from isolated matrix blocks during waterflood by establishing wetting phase bridges across open fractures in a mixed-wet, low-permeable, horizontally stacked chalk system. The established capillary continuity prolonged the viscous component in the water phase across the fracture and resulted in oil recovery exceeding the spontaneous imbibition potential by 10 %PV (Aspenes *et al*., 2008). In the case of waterflooding an oil-wet system, wetting phase bridges would not contribute to a viscous component across an open fracture as the oil phase would already be saturating the fracture. However, establishing capillary continuity between the two matrix blocks could improve oil recovery by eliminating the capillary end effect in the inlet matrix block. The different regimes of waterflooding a water-wet system and an oil-wet system thus call for different solutions to establish capillary continuity.

1.5 EOR from CO_2 injection

Injecting carbon dioxide (CO_2) into mature oil fields has several benefits which all have been studied over the past decades, including enhanced oil recovery (EOR), production of methane from natural gas hydrates and evaluating possibilities for underground CO_2 storage. Only the benefit of EOR from CO_2 injection will be discussed in this thesis. The impacts of accounting for different CO_2 properties such as viscosity and density and reporting various impacts of miscibility with n-Decane have been included.

CO_2 injection is a recognized EOR method due to its ability to easily dissolve into oil and thus reduce oil viscosity and extract light oil components (Abdassah *et al.*, 2000). The phase behavior of the reservoir oil and gas, depending on pressure and temperature, combined with the reservoir rock type, wettability and presence of fractures and their permeability, are crucial factors which determine the efficiency of the CO_2 injection. At sufficient density, CO_2 is able to displace most of the light ends of the hydrocarbons, and maintaining a high CO_2 pressure exceeding the Minimal Miscible Pressure (MMP) between the CO_2 and the oil in most of the reservoir throughout the recovery process thus yields a very high oil recovery.

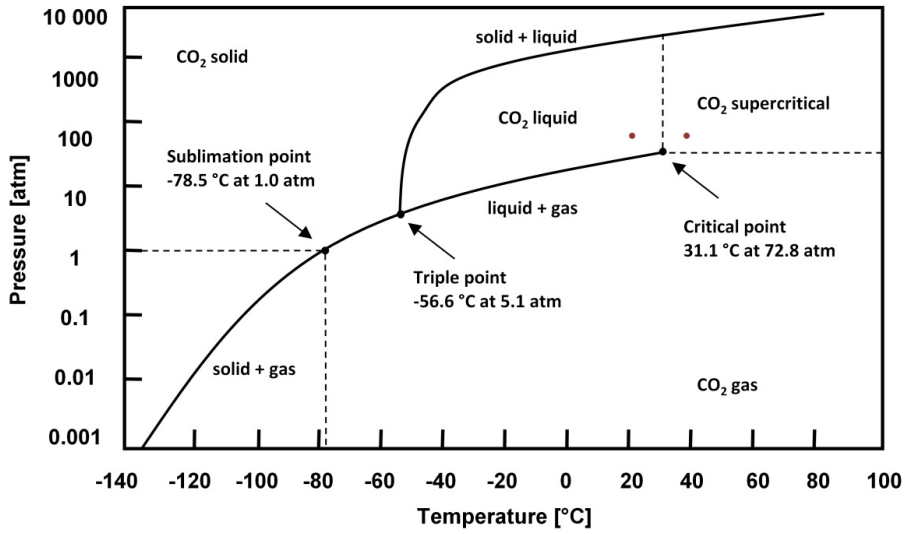

Figure 7: Phase diagram for CO_2, indicating the sublimation point, triple point and critical point. The two red dots at 81.7 atm and 23°C and 40°C indicate the operating conditions for the experiments performed in this thesis.

The CO_2 phase diagram is shown in Figure 7. The two red dots at 81.7 atm and 23°C (liquid CO_2) and 40°C (supercritical CO_2) indicate the operating conditions of the experiments in this thesis. CO_2 density and viscosity at different temperatures are shown in Figure 8 and Figure 9, respectively. At temperatures below the critical temperature (31.1°C), CO_2 density and viscosity increase rapidly when gaseous CO_2 is pressurized to obtain liquid state. At temperatures above the critical point, however, the gas/liquid boarder is not defined as a clear line, as indicated in the figures (Lemmon *et al.*, 2007).

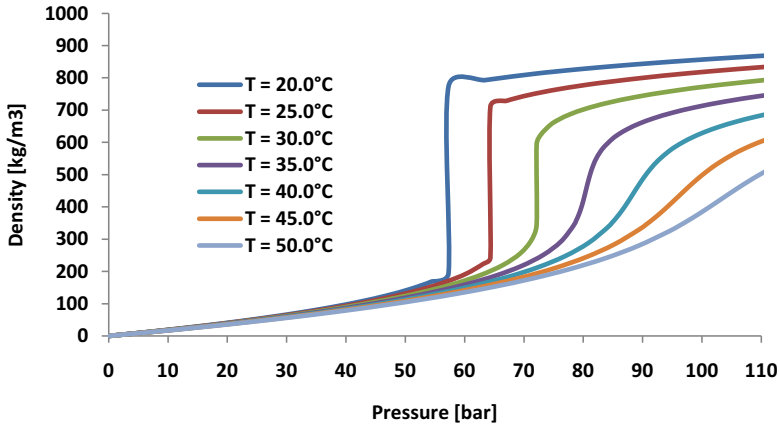

Figure 8: CO_2 densities as function of pressure at different temperatures (Lemmon et al., 2007).

In order to obtain good sweep efficiency, miscibility between CO_2 and the oil phase is a necessity. In a typical reservoir with a multi-component crude oil, the CO_2/crude oil MMP is a complex function which may change with temperature, reservoir depth and crude oil composition.

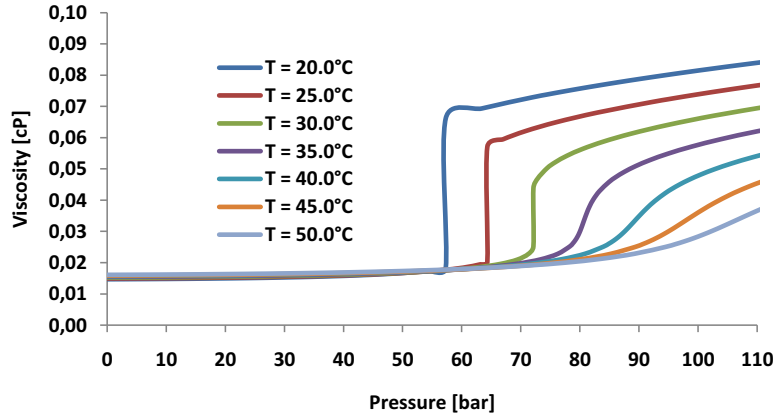

Figure 9: CO_2 viscosities as function of pressure at different temperatures (Lemmon et al., 2007).

In the lab, a simplified situation may be constructed to study CO_2/dead oil miscibility and displacement at constant temperature and pressure in core samples at different wettabilities and initial saturations. Maintaining a high pressure exceeding MMP is still a crucial condition for additional oil recovery. Interfacial tension as function of pressure at 37.8°C, 71.1°C and 104.5°C for a CO_2/n-Decane system is shown in Figure 10. The MMP at 37.8°C was determined at 79 bar using the VIT technique (Nagarajan and Robinson Jr, 1986, Ayirala *et al.*, 2005). Similar tests have reported MMP at 27.7°C well below 70 bar (Kulkarni and Rao, 2005a).

Miscibility is defined as the ability of two or more substances to form a single homogeneous phase when mixed in all proportions without the existence of an interface (Holm, 1986). If two fluid phases form after some amount of one fluid is added to the others, the fluids are considered immiscible and an interfacial tension (IFT) will exist between the immiscible phases. In a porous medium, the IFT between two immiscible phases will generate capillary forces which prevent complete displacement of one phase by the other. A substantial residual oil saturation will remain in the porous medium when injecting an immiscible fluid, e.g. water, to displace the oil. When displaced by a miscible fluid, however, the interfacial tension between the displaced and the displacing fluid is zero, and the residual oil saturation may decrease below 10 %PV.

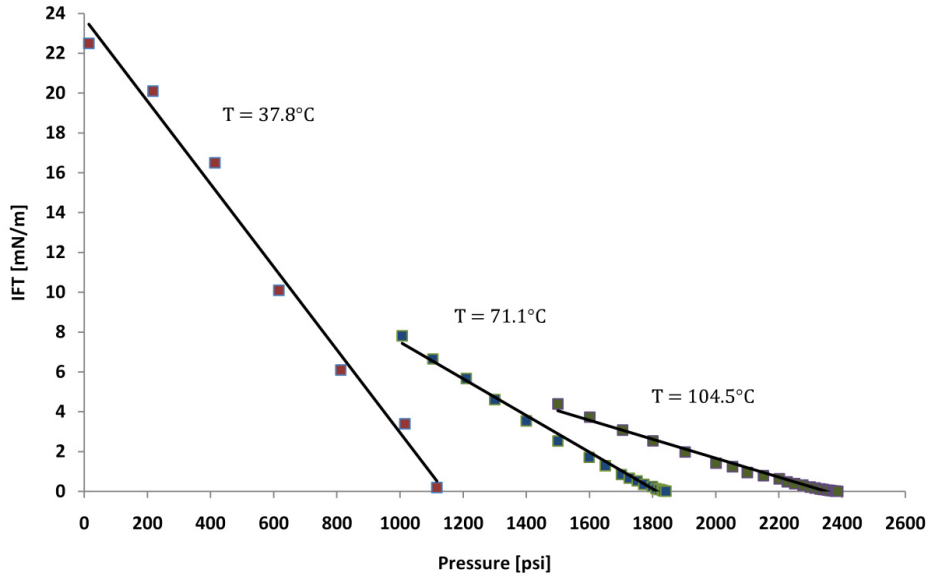

Figure 10: Interfacial tension as function of pressure at 37.8°C, 71.1°C and 104.5°C for a CO_2/n-Decane system. The MMP at 37.8°C was determined at 79 bar using the VIT technique (Nagarajan and Robinson Jr, 1986, Ayirala et al., 2005).

There are two types of miscible displacement; first-contact and multi-contact miscible displacement. In a first-contact miscible displacement, any amount of the solvent can be injected and will exist as a single phase with the oil in the reservoir. Low molecular weight hydrocarbons (propane, butane or mixtures of liquefiable petroleum gas) and heavier hydrocarbons (gasoline fractions) have been used as solvents for first-contact miscible flooding. Multi-contact miscible displacement is of two mechanistic types, vaporizing gas-drive and condensing gas-drive, both which include transfer of solvent or reservoir oil components to the other phase at the leading edge of the injected phase. The reservoir oil then becomes miscible with the freshly injected fluid. At reservoir conditions, highly compressed CO_2 extracts heavier components from the reservoir oil (gasoline-range) when injected as a liquid or supercritical fluid, making CO_2 a more efficient solvent than methane, nitrogen and flue gas.

Extensive research has been carried out on immiscible, near-miscible and multiple-contact miscible CO_2/oil displacement in porous media. Mangalsingh and Jagai reported on tertiary Continuous Gas Injection (CGI) and Water Alternating Gas (WAG) Injection in different CO_2/crude oil systems in water-wet sand packs under immiscible conditions. They found that the recovery was dependent on the WAG ratio (optimal at 1:4) and the injection rate, and that the optimal injection rates vary with the different crude oil compositions. CO_2 consumption, extraction of light components and oil viscosity alteration were also found to depend on oil composition (Mangalsingh and Jagai, 1996).

Shyeh-Yung studied the effects of pressure, initial saturations and volume of injected CO_2 in miscible and near-miscible displacement of oil by tertiary CO_2 injection in a CO_2/n-Decane system. The results indicated that oil recovery, oil bank size and CO_2 breakthrough time increased with pressure. The study concluded that oil recovery was improved by the diffusive capability of CO_2, which causes mass transfer even under immiscible and near-miscible conditions. Because of this mass transfer, oil can be recovered by oil swelling at lower pressures. A second conclusion drawn from the experiments addresses the fact that oil recovery during high pressure CO_2 injection well above MMP was not complete. The presence of initial water caused a water-shielding effect and oil bypassing which greatly reduced oil recovery (Shyeh-Yung, 1991).

Kulkarni and Rao published several papers on various methods of secondary and tertiary CO_2 injections at miscible and immiscible conditions. Their results indicated a significant increase in oil recovery for miscible floods over immiscible floods. While the immiscible flood recoveries (both CGI and WAG) were about 23%, the miscible floods provided 93.7% recovery for the CGI flood and 84.5% for the WAG flood regardless of the amount of CO_2 injected. They concluded that miscible gas floods were found to recover over 60% more of the waterflood residual oil than immiscible gas floods. They also found that the water shielding effect, responsible for delayed oil breakthrough in tertiary CO_2 floods, was minimal in the secondary WAG floods. However, the secondary CO_2 floods still provided a high oil recovery due to the higher initial oil saturation and capillary number than the tertiary CO_2 flood. Their work demonstrated that the optimal injection strategy consists of a combination of CGI and WAG using CO_2, and that the ultimate oil recovery is independent of whether the CO_2 injection is carried out as a secondary or tertiary process (Kulkarni and Rao, 2004, 2005a, 2005b).

In homogeneous, non-fractured reservoirs, CO_2 is an efficient EOR agent due to the properties reported above. In fractured or heterogeneous reservoirs, however, the efficiency of CO_2 injection is greatly reduced due to the presence of high permeable zones, allowing the CO_2 to bypass the matrix oil regardless of pressure, temperature and miscibility. Only a small percentage of the oil in the matrix will thus be contacted by the CO_2 in the fractures, and mass transfer will occur by molecular diffusion. As the oil dissolves the CO_2, the oil swells and produces into the fracture, resulting in enhanced oil recovery. Although some of the oil will dissolve the CO_2, swell and produce into the fracture, most of the oil remain trapped in the matrix blocks. In such cases, reducing the permeability of the fractures or high-permeable zones would be beneficial to divert the CO_2 from the fractures and into the matrix. Several experimental studies and successful reservoir projects have been reported on the matter (Hild and

Wackowski, 1999, Hughes *et al.*, 1999, Sydansk and Southwell, 2000, Karaoguz *et al.*, 2007). A specific example is given below.

In an experimental study reported by Chakravarthy *et al.*, CO_2 was injected at immiscible conditions as a tertiary EOR agent in fractured Berea sandstone. Due to its high mobility, the injected CO_2 channeled through the high-permeable zones, bypassing most of the residual oil in the matrix. To prevent this, a polymer gel was injected with the water phase to decrease the permeability in the fracture. The polymer gel saturated the fracture and solidified using a cross-link, creating a low-permeable gel in the fracture. During subsequent injection of CO_2, most of the oil in the matrix was contacted by the diverted CO_2 and was produced at the outlet or into the fracture, resulting in improved oil recovery. CO_2 injection in the presence of gel was found to recover an additional 10 %PV (Chakravarthy *et al.*, 2006).

Chapter 2. Experimental techniques and approaches

This chapter describes the core material and the different approaches and experimental techniques used in this thesis. The experimental techniques include the use of Magnetic Resonance Imaging (MRI) and embedded pressure ports to measure *in situ* saturation and pressure during continuous flooding. MRI was also utilized to study oil recovery mechanisms during injection of CO_2. In addition, NTI was used as a tool to study the impacts of capillary continuity on oil recovery in fractured core samples.

2.1 Core material and preparations

Outcrop rocks are commonly used in core flood experiments as analogues to reservoir rocks. Core samples collected directly from the reservoir can provide useful information to reservoir engineers, but the permeability and wettability of the cores are often damaged and the oil composition is complex and usually altered from the true reservoir oil. Collecting the quantity of reservoir core samples required for reproducible research purposes and laboratory studies would be very expensive and is not usually available. When reservoir rock samples are not available for systematic laboratory studies, similar outcrop rocks are used in a controlled environment to best represent the porosity, permeability, wettability and brine and oil composition of a given reservoir. In most of this thesis, Rørdal outcrop chalk (Ekdale and Bromley, 1993) from the Portland quarry at Ålborg in Denmark has been used to represent the Ekofisk reservoir rock in the North Sea. The Rørdal chalk is a homogeneous rock with high porosity (~50 %) and low permeability (~4 mD). The core samples were air evacuated and saturated with synthetic brine. Porosity was determined from weight measurements, and permeability to brine was measured using a biaxial Hassler core holder.

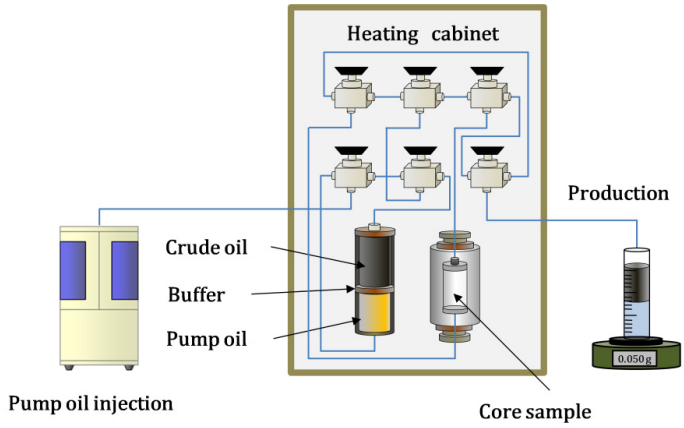

Figure 11: Schematic showing the setup for ageing core samples.

The selected outcrop rock must undergo certain modifications when used in laboratory experiments. The pore surface of outcrop rocks, which has never been contacted by crude oil, is strongly water-wet. The wettability conditions of most reservoir rocks

containing crude oil range from less water-wet to oil-wet, depending on rock mineralogy, pore-size distribution, oil composition and initial saturation. In order to alter the wettability conditions of the outcrop rocks used in the laboratory towards reservoir conditions, crude oil is flushed through the core at constant low rate at elevated temperatures for a selected period of time. Figure 11 shows a schematic of the setup used during ageing. Polar components in the crude oil break through the water film coating the pore surface and attach to the pore wall, creating areas of less water-wet or oil-wet conditions. As a measure of the average wettability condition of the core sample, the Amott Index is determined from the ratio of end-point saturations from spontaneous imbibitions and total recoveries:

$$I_{Amott} = I_w - I_o = \left(\frac{V_{si}}{V_{si}+V_f}\right)_w - \left(\frac{V_{si}}{V_{si}+V_f}\right)_o \quad (8)$$

where v_{si} is the volume produced by spontaneous imbibition of water (w) or oil (o) and v_f is the volume produced by viscous displacement. Further core preparations are conducted, including exchanging the water phase with radioactive brine for NTI experiments or deuterium oxide brine for MRI experiments.

2.2 *In situ* imaging

Extensive use of high spatial resolution Nuclear Magnetic Resonance (NMR) technology has been applied to obtain 2D and 3D visualizations of *in situ* fluid flow during the experimental work. The technology has a wide range of applications in modern science and research; in e.g. medicine and petroleum technology, Magnetic Resonance Imaging (MRI) is used for detailed 3D-imaging purposes.

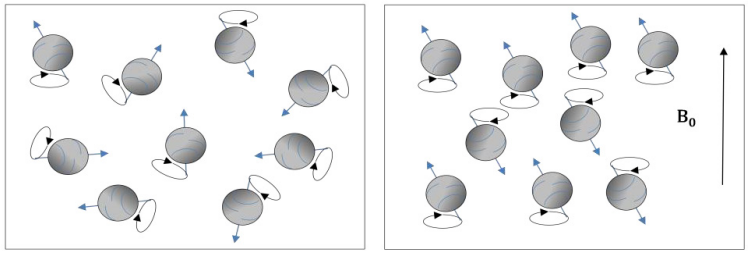

Figure 12: Precessing protons in absence (left) and presence (right) of a magnetic field B_0. *In presence of a magnetic field, each proton will align in one of two energy states as indicated to the right.*

In reservoir physics, NMR technology is used to measure fluid saturation distributions, to detect fluid movement, to identify displacement mechanisms, to measure *in situ* wettability conditions and to image core samples during flooding experiments. In this study, NMR Imaging has been used as a tool to study fluid flow during injection of liquid and supercritical CO_2 in low-permeable chalk at different wettabilities. A second set of experiments was constructed to measure *in situ* wettability indices, dynamic capillary pressures and relative permeabilities from local pressure and MRI saturation measurements.

The magnetic resonance property of nuclei was discovered in 1946 by two independent research groups (Bloch, 1946, Purcell *et al.*, 1946). Magnetic dipoles, such as hydrogen nuclei or protons, are associated with magnetic spin and magnetic moment. When placed in a strong magnetic field, these protons will precess around an axis parallel with the field in one of two energy states (Figure 12, right) according to quantum mechanics, causing a net magnetization of the protons.

Applied radio frequency fields corresponding to the difference between the energy states are used to systematically alter the alignment of the precessing axis and thus change the net magnetization. Resonant absorption of energy by the protons will occur at the Larmor frequency f_L for the particular nuclei:

$$f_L = \frac{\gamma \cdot B_0}{2\pi} \tag{9}$$

where $\gamma = 2.6752 \cdot 10^8 \frac{rad}{s \cdot T}$ is the gyro magnetic ratio for protons and B_0 is the strength of the applied magnetic field. When the radio frequency field is turned off, the excited protons return to the lower energy state and the magnetization to its initial state in a process called relaxation. During relaxation, each proton emits electromagnetic radiation which is detected by the MRI, and the strength of the signal is proportional to the amount of protons present in the sample. The signal can be manipulated by additional magnetic fields to build up enough information to construct 2D or 3D images. To do so, a number of smaller magnetic fields are applied around the core sample and changing the volume in which the resonance criterion is fulfilled. A more detailed description of MRI, relaxation, spin-echo detection and data acquisition has previously been published (Dunn *et al.*, 2002). In this thesis, deuterium oxide (D_2O) brine is used as the water phase and n-Decane is used as the oil phase. Deuterium oxide brine does not reveal any signal in the MRI at the current settings, and thus the detected MRI signal is assumed to be proportional to oil saturation. The typical spatial resolution of the MRI is 1 mm^3.

In addition to the NMR Imaging, the Nuclear Tracer Imaging (NTI) technique has been used to visualize fluid flow *in situ* during the experimental work. The method of approach is to label the water phase with a radioactive tracer which is immiscible to oil. The amount of γ-emitions from the radioactive tracer is proportional to the water saturation:

$$S_w^x = \frac{N_x - N_{BG}}{N_{100\ \%} - N_{BG}} \tag{10}$$

where S_w^x is the water saturation and N_x is the number of radioactive counts detected by a collimated Germanium detector (Figure 13) at position x along the length of the core, N_{BG} is the background radiation and $N_{100\ \%}$ is the number of radioactive counts at 100 % water/tracer saturation. By monitoring the radioactivity during drainage or waterflooding, the saturation distribution in the core sample may be calculated as a function of time. The typical resolution of the NTI method used during the experimental work is 1 cm.

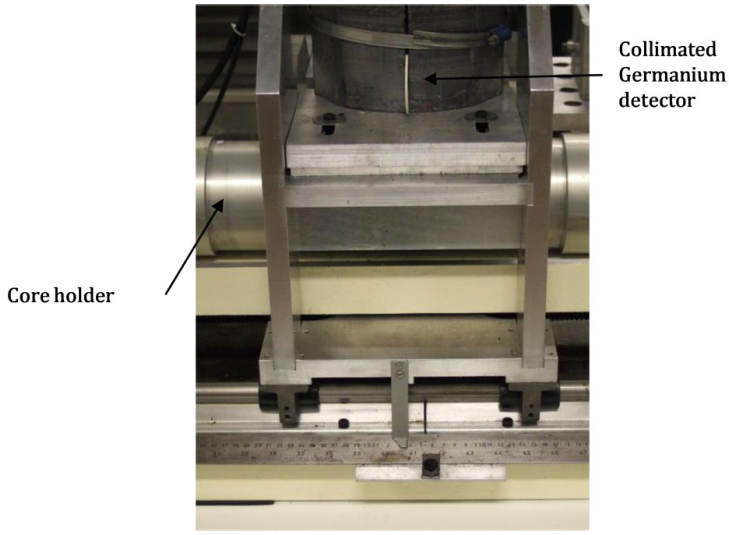

Figure 13: A Germanium detector is positioned above the core holder to obtain the number of γ –emitions from segments of the core.

2.3 Monitoring *in situ* dynamics during waterfloods

To prepare the core samples for the two phase *in situ* dynamics experiments, the cores, prepared at different wettabilities and saturated with D_2O brine and n-Decane at S_{wi}, were covered with epoxy, allowing fluid flow only through end pieces mounted at each end of the core samples.

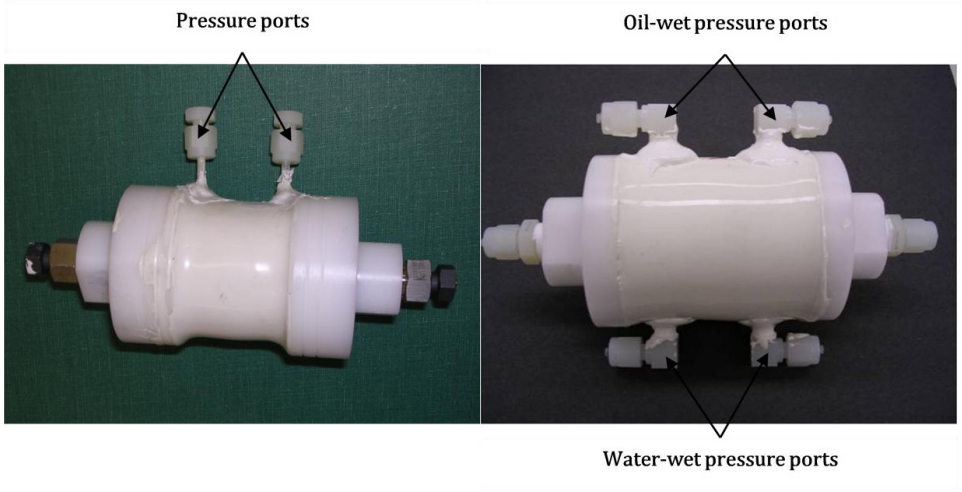

Figure 14: An epoxy-coated core with end-pieces and two embedded pressure ports mounted along the length of the core (left). An epoxy-coated core with four embedded phase specific pressure ports (right).

Only plastic fittings and end-pieces which reveal no signal in the MRI were used in two different pressure port setups during the experiments. The first setup included drilling two pressure ports into the core at selected positions along the length of the core as indicated in Figure 14 (left), allowing absolute pressure to be measured at two points inside the core during continuous flooding.

The second setup involved drilling four pressure ports into the core as indicated in Figure 14 (right). Keraflux™ semi-permeable discs with selected wetting preferences were embedded into the pressure ports and connected to pressure transducers. The pressure ports were sealed with silicone and a top layer of epoxy to prevent leakage. This allowed oil- and water pressures to be measured separately at two positions inside the core. A schematic of the experimental setup is shown in Figure 15. During injection of D_2O at low rates, high spatial resolution *in situ* saturation distribution data were monitored using MRI. Simultaneously, local absolute or phase specific pressures were logged as functions of time in the embedded pressure ports.

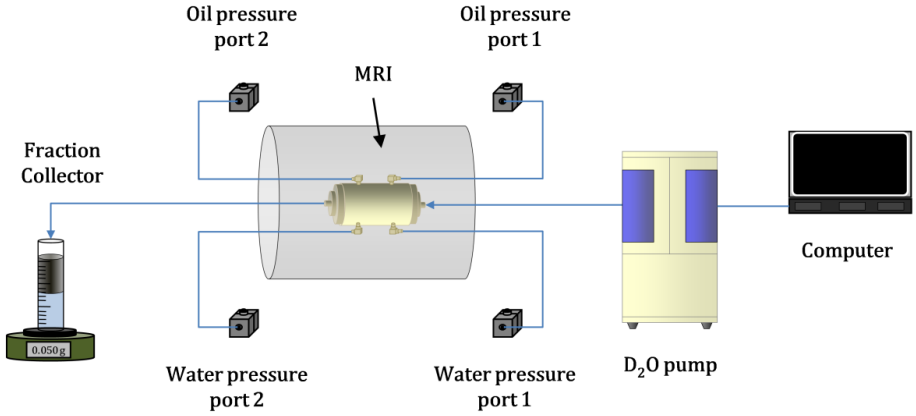

Figure 15: Schematic showing the experimental setup with phase specific pressure ports during the in situ *dynamics experiments.*

The collected data sets provided information to calculate *in situ* Amott indices, dynamic capillary pressure and relative permeability curves. To verify the key features of the experimental results, simulations were run using SENDRA core flood simulator developed at ResLab (http://www.ri.reslab.no/sendra.aspx). Production data, injection pressure and *in situ* saturation profiles collected from the experiments were used as input in the simulator to reproduce the *in situ* pressures.

2.4 Obtaining capillary continuity over fractures

An experimental setup was designed to study a reverse drainage process; i. e. oil injection in water-wet core samples was selected to represent water injection in oil-wet core samples. Two strongly water-wet core samples saturated with radioactive brine and separated by an open fracture defined by a 2.1 mm Teflon spacer, were placed in a biaxial Hassler core holder. Oil was injected at low constant pressure to establish a capillary end effect at the outlet end of the inlet core. During the oilflood,

fluid saturation distributions were continuously monitored using a Germanium detector. When brine production from the inlet core terminated, the outlet core was removed from the core holder, and the fracture was packed with water-wet, fine-grained particles.

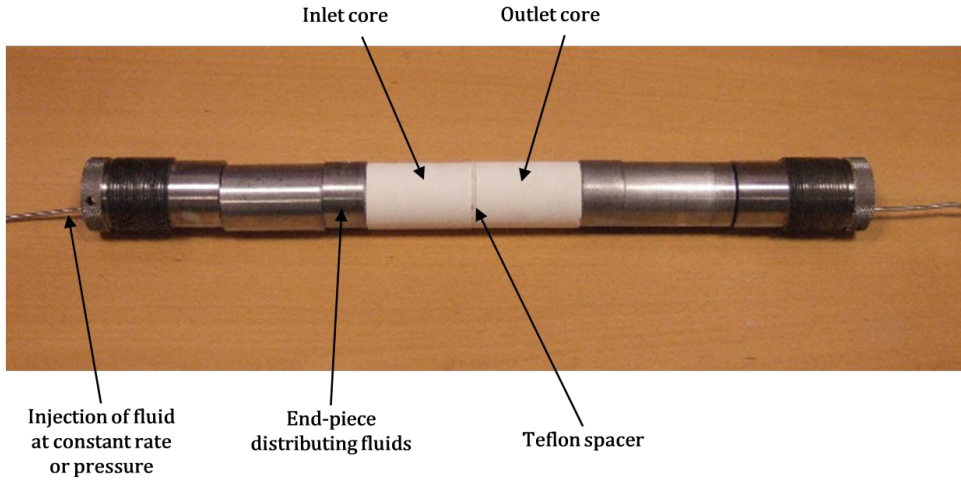

Figure 16: Stacked core plugs separated by an open fracture using a 2.1 mm Teflon spacer ring. The system was mounted into a biaxial core holder, and a slight confinement pressure was imposed.

Table 1. History of the experimental procedure for oilflooding the strongly water-wet, stacked core plugs separated by a 2.1 mm fracture.

Differential Pressure [psi]	Fracture Content (mm)	Injection Time/Volume
20	Open with fluid	4 hours
30	Open with fluid	30 hours
60	Open with fluid	26 hours
60	Open with fluid	2 hours
60	Broken glass (0.5 - 1.0)	2 hours
60	Broken glass (0.5 - 1.0)	5 hours
60	Sand (0.5 - 1.0)	3 hours
120	Sand (0.5 - 1.0)	1 hours
120	Sand (0.125 - 0.250)	1 hours
120	Sand (0.125 - 0.250)	24 hours
120	Sand (0.125 - 0.250)	24 hours
120	Sand (0.125 - 0.250)	500 ml
120	Fine-grained chalk	500 ml

Particle packing used in the three subsequent studies reported were broken glass, coarse or fine sand and crushed, fine-grained chalk, respectively. The outlet core was

reassembled into the Hassler core holder, and oil was subsequently injected using the same constant pressure. Figure 16 shows two stacked core samples separated by a 2.1 mm Teflon spacer. Various differential pressures were applied for the different particle fillings to determine the effects from fracture permeabilities. An experimental history of injection pressures, duration for each oilflood and specification of fracture filling for each experiment is listed in Table 1.

Similarly to the strongly water-wet experiment, two stacked core samples were placed in a Hassler core holder separated by a 4.2 mm open fracture, using a moderately water-wet core sample as the inlet plug to represent a drainage process in a less oil-wet core sample. The increased fracture aperture was applied to prevent wetting phase bridges to form across the open fracture (Aspenes *et al.*, 2008). An experimental history of injection pressures, duration for each oilflood and specification of fracture filling for each experiment are listed in Table 2.

Table 2. History of the experimental procedure for oilflooding the moderately water-wet, stacked core plugs separated by a 4.2 mm fracture.

Differential Pressure [psi]	Fracture Content (mm)	Injection Time
60	Open with fluid	24 hours
120	Open with fluid	24 hours
Waterflood with radioactive brine to S_{or}		
60	Open with fluid	6 hours
60	Broken glass (0.5 - 1.0)	48 hours
90	Broken glass (0.5 - 1.0)	27 hours
Waterflood with radioactive brine to S_{or}		
10	Open with fluid	27 hours
20	Open with fluid	22 hours
20	Broken glass (0.5 - 1.0)	18 hours
40	Broken glass (0.5 - 1.0)	2 hours
40	Broken glass (0.5 - 1.0)	120 hours

Two Edwards limestone core plugs from the Edwards formation, New Mexico, prepared at slightly oil-wet conditions and saturated with radioactive brine and residual oil, were placed in a Hassler core holder separated by a 4.2 mm open fracture. One mobile pore volume of oil and one mobile pore volume of radioactive brine were successively injected at constant rate 0.4 ml/h to establish capillary end effects at the outlet end of the inlet core plug. The outlet core was removed from the core holder, and the 4.2 mm Teflon spacer was replaced by a 1.0 mm Teflon spacer. The injection sequence was repeated at the same constant rate, and a third flooding sequence was conducted at the same constant rate with the 1.0 mm fracture being packed with fine-grained oil-wet particles denoted PMMA355. A detailed history of the experiments is listed in Table 3.

Table 3. History of the experimental procedure for the slightly oil-wet, stacked core plugs.

Fracture Width [mm]	Injection Rate [ml/h]	Phase / PV Injected	Fracture Content
4.2	0.4	Brine / 0.26	Open with air
4.2	0.4	Oil / 0.26	Open with brine
4.2	0.4	Brine / 0.26	Open with fluid
1.0	0.4	Brine / 0.26	Open with air
1.0	0.4	Oil / 0.26	Open with brine
1.0	0.4	Brine / 0.26	Open with fluid
1.0	0.4	Brine / 0.26	PMMA355 with air
1.0	0.4	Oil / 0.26	PMMA355 with brine
1.0	0.4	Brine / 0.26	PMMA355 with fluid

Two strongly water-wet Bentheim sandstone core samples from the Bentheim quarry in Lower Saxony, Germany, were cut in two and vertically stacked. Using 2.1 mm Teflon spacers to separate the core pieces, the two systems were epoxy-coated and saturated with brine. In one of the systems, the fracture was packed with fine-grained crushed Portland chalk. During air-brine gravity drainage using a closed loop at water vapor pressure, the NTI technique was applied to monitor the fluid saturation distributions and to study the impacts from capillary continuity on the capillary end effects.

2.5 CO_2 injection at miscible conditions

A number of core samples saturated with D_2O brine and n-Decane at different wettabilities were placed in the MRI and pressurized to 82.7 bar (1200 psi) with a 103.4 bar (1500 psi) confinement pressure. At 82.7 bar, CO_2 is at liquid state at room temperature (~25°C) and becomes supercritical at temperatures above the critical point (31.1°C). CO_2 is first-contact miscible with n-Decane at 82.7 bar and below 40°C (Ayirala *et al.*, 2005).

The cores were mounted with shrink tubing in a fiberglass Temco core holder, specially constructed for high pressure experiments at elevated temperatures, MRI imaging and CO_2 flooding. Fluorinert (FC-40) was circulated through the confining space in the core holder and a refrigerating bath with constant temperature using a reciprocating pump at constant pressure. The fluorinert thus acted as a confining and temperature controlling liquid. A schematic of the setup is shown in Figure 17.

A series of CO_2 injection experiments were conducted in fractured and non-fractured core samples, varying parameters such as wettability, initial saturations and temperatures at secondary and tertiary conditions. Continuous monitoring of the 3D *in situ* fluid saturation distributions provided qualitative data to study local fluid flow behavior and recovery mechanisms.

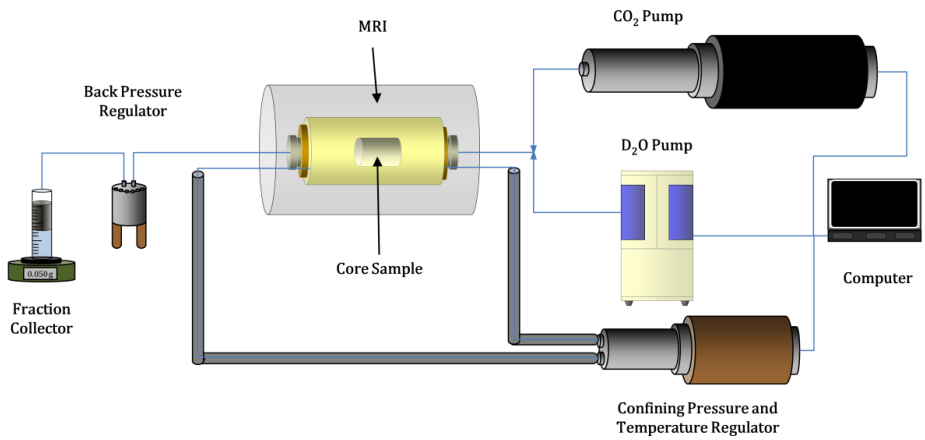

Figure 17: Schematic showing the setup for CO_2 experiments.

Chapter 3. Results and discussions

The main results and applications from *in situ* saturation and pressure measurements during waterflood of low-permeable chalk are presented in the following. The applications include calculation of dynamic capillary pressure and relative permeabilities at different wettabilities, *in situ* Amott-Harvey Indices of wettability and enhanced oil recovery potential from establishing capillary continuity over fractures. In addition, the studies of CO_2 injection as an EOR agent at liquid and supercritical conditions above MMP using MRI are presented. The scientific papers included in this thesis are listed in the "**List of publications**" chapter on page *viii*.

3.1 Dynamic capillary pressure and relative permeability curves

The common way of expressing capillary pressure in porous media is given by:

$$p_c = p_{nw} - p_w = f(S) \tag{11}$$

where p_c is the capillary pressure, p_{nw} is the pressure in the non-wetting phase, p_w is the pressure in the wetting phase and *f(S)* is a function of saturation. It is generally assumed that the expression for capillary pressure accounts for all the effects that influence the equilibrium distribution of fluids, such as surface tension, presence of fluid-fluid interfaces, wettability of solid surfaces, grain size distribution and micro-scale heterogeneities (Hassanizadeh *et al.*, 2002). In addition to the effects mentioned above, it is a well known fact that the capillary pressure (and the relative permeability) is dependent on the fluid dynamics; saturation history, known as capillary pressure hysteresis, and the rate of change of the saturation. The latter effect is not well understood or properly quantified, but several suggestions for adding a dynamic term to the definition of capillary pressure are presented in the literature. In general, the dynamic capillary pressure is larger than the static capillary pressure for drainage processes and smaller for imbibition processes (Hassanizadeh *et al.*, 2002).

The conventional methods for calculating capillary pressure involve saturation and pressure measurements at equilibrium state. The conventional methods include the centrifuge technique, the mercury injection method and the porous plate technique (Anderson, 1987a). Several other non-conventional techniques are presented in the literature, including the direct measurement of saturation method (DMS), the desorption of water vapor method and the semi-dynamic method. ***Paper 1*** demonstrates capillary pressure measurements during continuous waterflooding, as opposed to the conventional steady-state methods.

One of the main challenges in the experiment was to obtain accurate pressure readings in each of the pressure ports. Using the MRI to measure *in situ* saturations prevented the use of any metallic, electric or magnetic objects close to the MRI instrument. The pressure transducers used to measure the five different pressures; the inlet pressure and two different water and oil pressures, were thus connected to the core using plastic tubing and placed on a table five meters away from the MRI magnet. The plastic tubing was filled with water or oil to establish fluid continuity from the core to the transducers and to prevent any time delay in the pressure response. It proved difficult,

however, to obtain correct initial conditions in the experimental setup, and some of the pressure readings were consequently negative during parts of the waterflood.

A second challenge was to transform MRI intensities into exact saturation values in the pressure ports. In some cases, 3D images were collected of the whole core sample during continuous injection, and the linear relationship between MRI intensity and oil saturation calculated from end-point production data was used in the pressure ports. In other cases, transverse 2D images were collected at the pressure ports, and sagital or coronal images were collected to obtain average saturations in the core. Due to different MRI settings in the sagital/coronal and transverse images, the linear relationship used to obtain average core saturation values did not translate directly into pressure port saturations. Thus, the pressure port saturations were calculated using the coronal or sagital images, but with less spatial accuracy. Alternatively, the pressure port saturations were calculated from the transverse images assuming uniform end-point saturations.

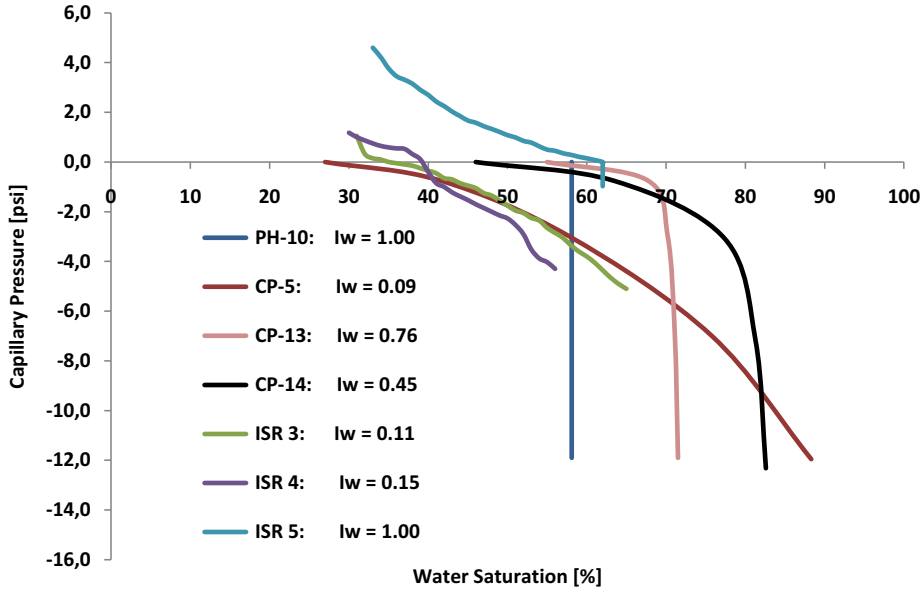

Figure 18: Capillary pressure curves from conventional centrifuge measurements (Graue et al., 1999) compared with the results presented in ***Paper 1****.*

As discussed in the paper, the two phase pressures are collected at the same saturations, and capillary pressures at different wettabilities are calculated according to the definition. The results are compared to similar capillary pressure curves (Figure 18) obtained from the conventional centrifuge method (Graue et al., 1999).

Paper 1 summarizes the results from two distinctively different sets of experiments. Measuring the local *in situ* pressures (without semi-permeable discs) and fluid saturation distributions using MRI during continuous constant pressure waterfloods in the first set of experiments provided data to identify the separate contributions from spontaneous and viscous displacement and to calculate the *in situ* Amott indices. The

method for calculating the Amott indices was further elaborated and investigated in ***Paper 2***, demonstrating consistency, reproducible accuracy and confirmation of the conventional wettability measurement methods.

The second set of experiments included pressure measurements with semi-permeable discs installed in the pressure ports, allowing separate phase pressures to be monitored during waterfloods. It could be debated whether the monitored phase pressures show the true water and oil pressures separately, or if each of the measured phase pressures is under the influence of the other phase.

A few indications are presented, showing that the semi-permeable discs only respond to changes in the respective phase: Starting at irreducible water saturation, water is injected at the inlet, and only the oil phase is mobile. This is reflected in the immediate response in the oil pressure ports, while the water pressures remain at the initial states. As the water injection progress, the water phase is mobilized, and the water pressures are increasing accordingly with an expected time delay between Port 1 and Port 2 (Figure 19). Based on these indications, and to continue with the capillary pressure and relative permeability calculations, it was assumed that the pressure ports were monitoring each fluid phase pressure separately and with no influence from the other fluid phase.

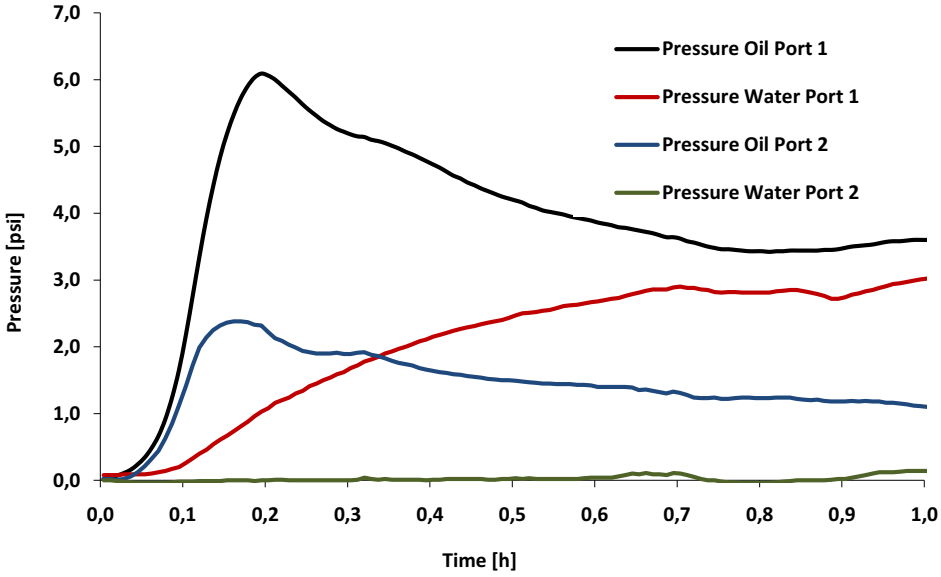

Figure 19: The pressure response in the oil pressure ports (black and blue lines) and in the water pressure ports (red and green lines) in Port 1 and Port 2 during the first hour of injection in core sample ISR 5, respectively.

The results from the second set of experiments were used to calculate *in situ* capillary pressures and relative permeabilities *dynamically*, as opposed to the conventional steady-state methods. The obtained capillary pressure curves were compared to conventional centrifuge data, demonstrating consistency with the expected results.

3.2 Direct calculation of relative permeability

The relative permeability curves obtained from the *in situ* pressure and saturation data and reported in ***Paper 1*** were calculated using an explicit method (Kolltveit *et al.*, 1990) and showed a significant disagreement with the conventional data. A further investigation of the calculation method was initiated, and the new experiments using constant rate injection reported in ***Paper 3***, combined 3D fluid saturation imaging and a slight modification to the equations used in the calculations.

The improved method provided more reliable relative permeability curves. Figure 20 show the oil and water relative permeabilities in a strongly water-wet core sample obtained from the modified calculation method, compared with a set of relative permeability curves from a modified Penn state method using *in situ* saturation measurements and avoiding capillary end effects (Graue et al., 1999). A sensitivity analysis with respect to the Darcy velocities is also given in ***Paper 3*** and shown in Figure 20 as the red and green lines, indicating over- and underestimations of the Darcy velocities.

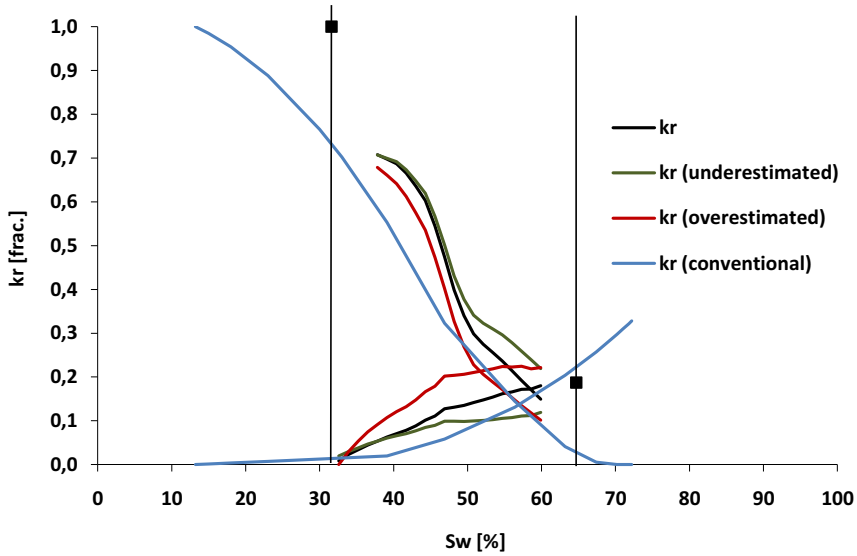

Figure 20: Relative permeabilities for core plug ISR 5 (I = 1.00) calculated from the in situ *data (black line). The red and green lines are calculated based on the over- and underestimated Darcy velocities, respectively. The blue lines are relative permeabilities from conventional steady-state methods (Graue et al., 1999), and the black dots indicate end-point relative permeabilities.*

The main modification to the method included the assumption that the Darcy velocity in the water phase in one of the pressure ports was linear with saturation. From the equation of continuity and the *in situ* saturation profiles, the assumption proved reasonable during most of the experiments. The Darcy velocity of the oil phase was calculated by subtracting the Darcy velocity to water from the injection rate.

3.3 *In situ* Amott-Harvey indices

A technique for measuring Amott-Harvey indices of wettability during continuous waterflooding at constant pressure is reported in ***Paper 2***. The results corroborated the conventional Amott Index measurement technique, which is based on measuring the volumes of oil and water produced during spontaneous imbibition and subsequent forced flooding. The key element in wettability measurements is to identify the average saturation at zero capillary pressure. In the conventional method, zero capillary pressure is reached at the end-point for spontaneous imbibition. Continued injection provides the additional recovery from forced waterflood, and the Amott Index may thus be calculated. Obtaining the wettability data using the conventional method may take up to a month at less water-wet or at intermediate wettability conditions, compared to a few days of continuous injection at low rate in the method proposed in ***Paper 2***.

Table 4: In situ *Amott Indices of wettability compared to conventional data.*

Core Name	Conventional Amott Index [frac.]	*In situ* Amott Index [frac.]	Difference [frac.]
M3	0.39	0.51	0.12
M8	0.45	0.48	0.03
E4	0.17	0.21	0.04
T3	1.00	0.98	- 0.02

In situ Amott Indices were measured during continuous waterfloods at constant pressure injection by using simultaneous *in situ* fluid saturation and local pressure measurements. Using the pressure curve to identify the spontaneous imbibition and forced waterflood regimes, the recovery contributions from spontaneous imbibition and viscous displacement are measured and used to calculate the local Amott Indices directly. Amott Indices were measured at two different positions in each of the core samples to demonstrate reproducibility and summarized in Table 4.

3.4 Establishing capillary continuity over fractures

During drainage processes in stacked core samples at different wettabilities, separated by a fracture packed with different wetting phase particles, the capillary end effect was monitored during continued injection to determine if capillary continuity had been established. As reported in ***Paper 4***, packing the fracture with crushed, fine-grained chalk in the strongly water-wet, horizontally stacked case resulted in an estimated 5.6 %PV additional recovery of the wetting phase. Additional recovery from packing the fracture with glass or sand particles was not detectable using the Nuclear Tracer Imaging technique. In the slightly oil-wet case, an additional 4.3 %PV of oil was recovered when the fracture was packed with oil-wet micro-particles PMMA355. During gravity drainage in a brine-air system of vertically stacked, strongly water-wet sandstone with open fracture, brine production from the inlet core was estimated to 15 %PV. By packing the fracture with strongly water-wet, crushed chalk, the entire volume of water captured by the end effect was produced during continued drainage and increasing brine production with an estimated 65 %PV (Figure 21).

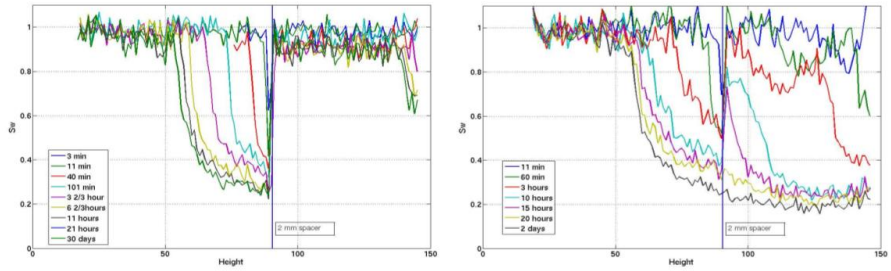

Figure 21: Water saturation distributions in vertically stacked, strongly water-wet sandstone during gravity drainage with an open fracture (left) and with the fracture packed with crushed chalk (right). Capillary continuity was obtained (right), and the volume of the wetting phase otherwise captured by the capillary end effect was produced.

One of the key assumptions made during the analysis of the results was to assume full saturation of the injected fluid in the fracture after 1 PV of injection. Due to the strong impact from the radioactive brine in the open fracture to the fluid distribution measurements in the inlet core plug, determining whether a spike in the saturation measurements was due to radioactive brine in the fracture or the actual capillary end effect had great impact on the analysis of the results and on determining the next step in the experiment.

Parts of the conclusions in the paper state that using different *in situ* measurement techniques such as MRI or CT would complement the results using nuclear tracers and possibly verify or disprove the results and avoid the strong background noise from the radioactive brine in the fracture. In addition, using MRI or CT would greatly improve the spatial resolution of the measurements in the vicinity of the fracture, allowing further investigation of the experiments and determination of the recovery mechanisms across the fracture at different wettabilities.

Obtaining capillary continuity from manually packing the different particles in the fracture proved difficult to reproduce, and an automated particle packing or injection procedure to establish a certain amount and packing pressure would thus be favorable. Disabling the confinement pressure surrounding the core, which was necessary in order to remove the outlet core and fill the fracture with particles, may alter the saturation distribution in the cores significantly. In the results presented in ***Paper 4***, an initial fluid saturation profile was always obtained before continuing with the injection.

During the different stages of the experiments reported in ***Paper 4***, a number of fracture filling particles were used: The glass particles were crushed, water-wet pipette glass, sieved to reach particle size between 0.5 and 1.0 mm. The water-wet sand particles were between 0.5 and 1.0 mm (coarse-grained sand), and between 0.125 and 0.250 mm (fine-grained sand). Changing from glass to sand particles was initiated to increase the total contact area between the inlet core sample and the fracture particles, possibly boosting the matrix-fracture transport due to the porosity and capillarity of the sand particles. The crushed, fine-grained chalk particles were finally packed in the fracture to further increase the contact area and to make use of the high capillarity of the chalk.

Using the NTI technique, additional recovery from the inlet core sample was detected during continued flooding in the strongly water-wet case, but it was concluded from the results that capillary connectivity had not been established due to the continued presence of capillary end effects. Finally, introducing crushed, high capillary Rørdal chalk particles between 0.5 and 1.0 mm in size established capillary connectivity across the fracture, recovering the volume captured by the capillary end effects. The importance of the fracture filling being porous and highly capillary itself, proved to be eminent.

3.5 EOR from CO_2 injection

CO_2 is a well known EOR agent used in many oil fields worldwide. Its capability to mix with reservoir oil, extracting light oil components and making the oil less viscous contributes to increased mobility and enhanced oil recovery during WAG or CO_2 injections. In ***Paper 5***, the *in situ* recovery mechanisms are investigated by monitoring the fluid saturation distributions using MRI during secondary and tertiary injections of liquid or supercritical CO_2 at different wettabilities.

One of the key features observed during injection of CO_2 in the porous medium, was a distinct increase in the MRI signal as CO_2 was introduced to the system. An example of this effect is shown in Figure 22. At a very early stage in the CO_2 flood, even before any additional oil was recovered, an increase in the MRI signal at the inlet side of the core was detected. The high MRI intensity area then advanced through the core, after which the remaining signal approached zero as indicated in Figure 23.

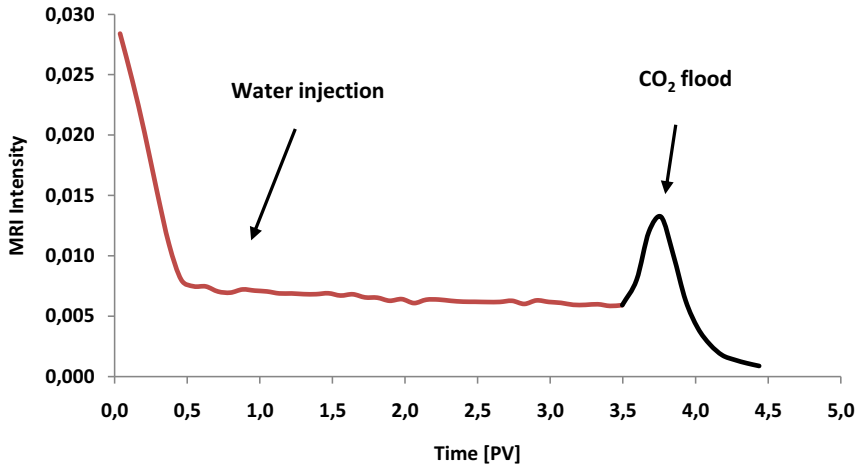

Figure 22: MRI intensity as function of injected pore volume during waterflood (red line) and subsequent CO_2 flood (black line).

Figure 22 and Figure 23 show the average MRI intensity and the images obtained from only one of the core samples used in this study, but they illustrate the general trend observed during all the tests. In some cases, the MRI intensity approached zero with

25 %PV oil left in the core. Previous research has shown a linear relationship between MRI intensity and oil saturation during waterfloods in Rørdal chalk. This was tested by comparing the average MRI intensity with the saturations based on material balance. The measurements were quantitative and the oil saturation may therefore be calculated in blocks or regions of interest of the core wherever water is displacing oil. For CO_2 floods, however, no such correlation is established. The NMR properties of CO_2/n-Decane mixtures are complex and beyond the scope of this thesis, but a few explanations of the observed MRI intensities are suggested below.

During waterflood in a water-wet brine/n-Decane/matrix system it is assumed that most of the oil phase will be surrounded by water and bulk relaxation of hydrogen will be dominating. Hydrogen will experience the same environment throughout the waterflood as the oil phase and the water phase do not mix. During a subsequent CO_2 flood, however, the relaxation properties may change with time as the oil phase mix with CO_2 and as a consequence the T_1 and T_2 relaxation times may change. A test was designed to study the NMR T_2 properties in bulk at different concentrations of CO_2 and n-Decane in a 2 MHz instrument, but no change in T_2 was observed. It could be argued, however, that performing the same test in a porous medium in the 85.7 MHz MRI instrument would incorporate influence from both diffusion and matrix minerals. It is not intuitive, however, that the initial increase in MRI intensity is overlapped by a decrease of signal as phase mixing continues. There is no reason to expect that there are more or fewer H^1 nuclei in the system due to the swelling and change of density. Assuming that hydrogen nuclei in pure n-Decane is not fully polarized, this would lead to more signal if T_1 decreases when CO_2 mix with n-Decane. Increased polarization due to T_1 enhancement may explain the initial increase in MRI signal shortly after CO_2 is injected. If this is true, one can argue that the signal will increase to a point where T_1 is short enough to get close to complete polarization. Additional decrease in T_1 would not add more signal after this point. The MRI requires a polarization time of about $5 \cdot T_1$ to achieve full polarization (equilibrium). As for the T_1 relaxation time, the MRI signal will also be affected by the spin-spin relaxation time T_2. However, the signal intensity will vary with T_2 in a continuous way until the T_2 is below 2-3 ms, where no signal can be detected. This might explain the continuous decrease as seen after the initial signal increase.

Another explanation for increased MRI signal may be related to swelling of the oil phase when mixing with CO_2, which is a well reported phenomenon in the literature. Some of the oil trapped in the smaller pores, preferably close to the pore walls in a less water-wet medium, may be mobilized during CO_2 injection by swelling and transferred to larger pores where fast surface relaxation is less dominant. In this case the effect should be more prominent in less water-wet system, where more of the oil phase is coating the pore surface.

The third effect may be a result from increased self-diffusion of hydrogen spins as the oil phase is diluted by CO_2. Due to local inhomogeneities in the static magnetic field B_0 the diffusing spins will be precessing with slightly different Larmor frequencies and the system will lose phase coherence and reveal lower signal. The average MRI intensity will decrease, and even approach zero as the oil is further diluted. This may also explain the fact that the MRI signal continues to decrease at residual oil saturation – when no more oil is produced.

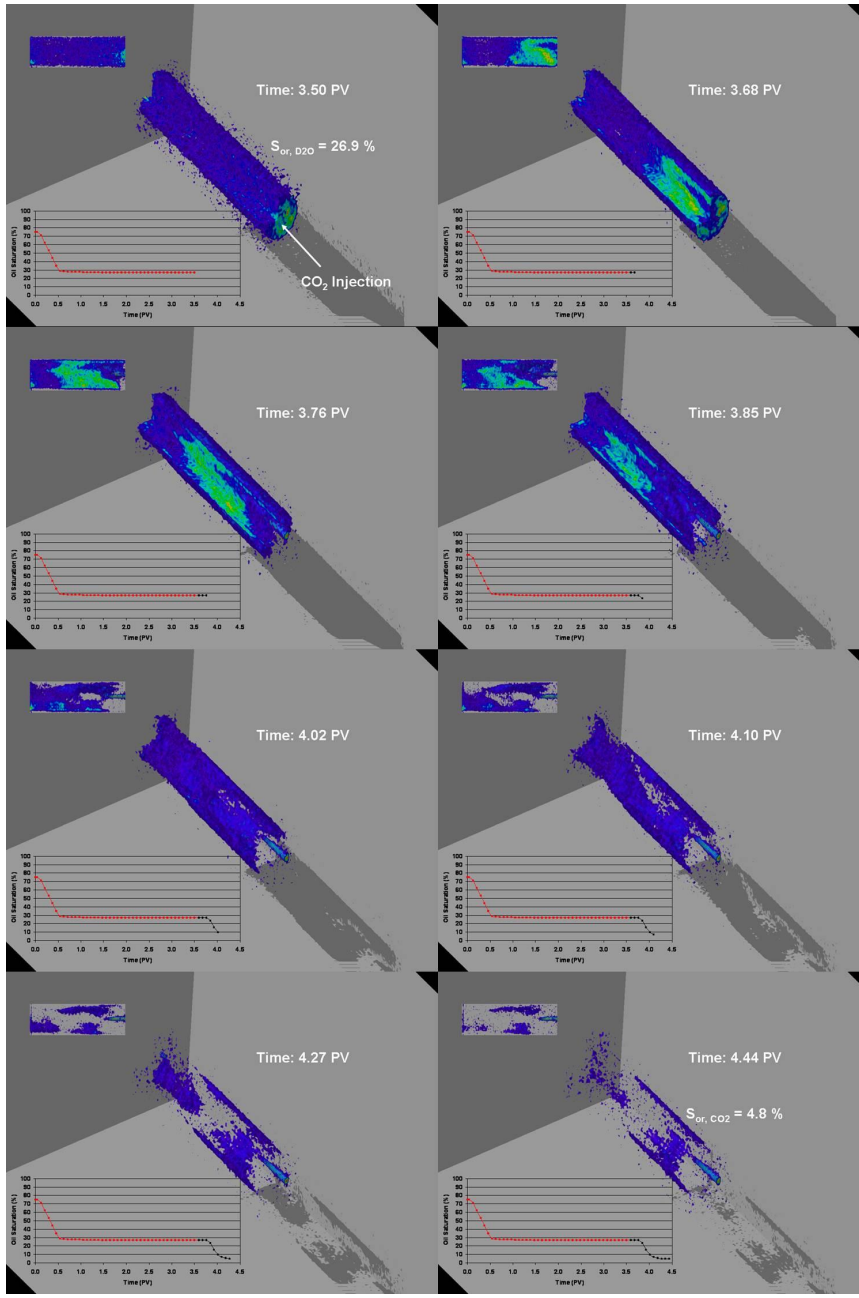

Figure 23: A series of MRI images obtained during injection of CO_2. A high intensity area advances through the core and leaves only a minimum of detectable signal left.

Although these effects hampers the local measurements by means of quantity, it might, with further work and understanding of the mechanisms involved, provide additional and valuable information of how CO_2 mix and diffuse in oil and water saturated porous

media. Measurements of relaxation times in addition to conventional spin-echo imaging would be the first suggestion for further work.

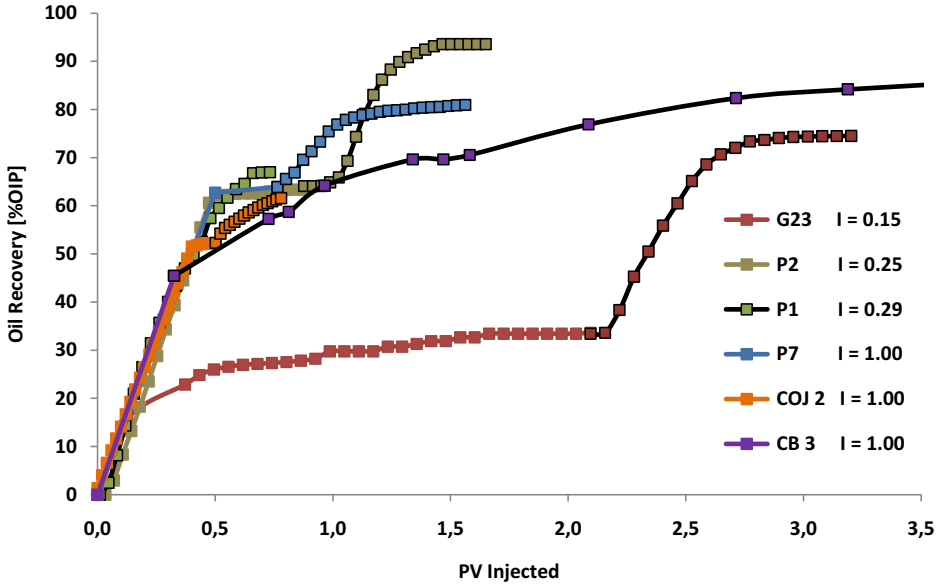

Figure 24: Oil recovery from waterflooding and subsequent injection of CO_2 in five core samples, and recovery from the sixth core sample (P1) during secondary injection of CO_2. Amott Indices as denoted in the legend.

An extended discussion of the oil recovery from waterflooding and subsequent injection of CO_2 was given in ***Paper 6***. A summary of the recoveries as function of injected pore volumes is given in Figure 24. A thorough discussion regarding the impact from wettability, initial saturations and injection of CO_2 at secondary, tertiary, liquid and supercritical conditions on oil recovery was also given in the paper. Similar to ***Paper 5***, the MRI images in ***Paper 6*** were only used as a tool to describe *in situ* fluid flow qualitatively, as the ability to quantify *in situ* saturations were limited.

In addition to the previously reported results, waterflooding and subsequent injection of CO_2 in a fractured, strongly water-wet core sample monitored in the MRI was demonstrated in ***Paper 6***. The qualitative analysis of the MRI images showed block-by-block displacement during waterflood and only minor oil recovery from the middle and outlet core pieces during injection of CO_2. The images indicated that most of the oil in the matrix was not contacted by the CO_2, and that fluid flow was located in the fracture network, resulting in early CO_2 breakthrough and low enhanced oil recovery. This corroborates the results from previous work (Chakravarthy *et al.*, 2006).

Conclusions

Complimentary *in situ* saturation imaging techniques have been used to measure fundamental parameters such as relative permeability, capillary pressure and wettability and the impacts from capillary continuity across fractures on oil recovery. The basic parameters control the fluid distribution and describe fluid flow properties in porous rocks, and knowledge of transport mechanisms in fractured systems is essential in realistic reservoir production scenarios. Finally, *in situ* imaging was used to investigate fluid flow during enhanced oil recovery by injection of CO_2.

A method for calculating dynamic capillary pressures in porous media from *in situ* saturation and phase pressure measurements has been demonstrated at different wettabilities and compared to conventional data. As opposed to capillary pressure curves generated from the centrifuge or mercury injection methods, which rely on pressure or saturation equilibrium, the data from the proposed technique are collected during continued injection using Magnetic Resonance Imaging to obtain *in situ* saturation distributions and semi-permeable discs to measure local phase pressures. The obtained capillary pressure curves demonstrated consistency and reproducibility at strongly water-wet, less water-wet and neutral-wet conditions.

Relative permeability curves have been generated using an explicit calculation method, which utilizes *in situ* fluid saturation and phase pressure data obtained during continuous waterfloods. The method has been reviewed and slightly modified to match the generated data set, and demonstrates a good match with conventional relative permeability curves at strongly water-wet conditions.

Amott-Harvey indices of wettability have been obtained from simultaneous pressure and saturation measurements during continuous injection of water at constant pressure and calculated by identifying the separate recovery contributions from spontaneous imbibition and forced waterflood. The most important features from the experiments have been verified by numerical simulations, and the Amott-Harvey indices showed excellent coincidence compared to the conventional measurements.

An experimental setup was designed to determine if capillary continuity across an open fracture could be obtained by filling the fracture with micro-particles. Using the NTI technique, the volume of the wetting phase captured by the capillary end effect was monitored during continuous flooding, and it was concluded that capillary continuity was obtained in the strongly water-wet systems when packing the fractures with water-wet, crushed chalk particles. In the slightly oil-wet case, impact from packing the fracture with oil-wet micro-particle was detected, but it could not be concluded that capillary continuity had been obtained due to the accuracy of the measurements.

In a series of experiments, MRI was used to monitor *in situ* saturation distributions and to study recovery mechanisms during injection of CO_2. At different wettability conditions and initial saturations, injecting liquid or supercritical CO_2 at secondary or tertiary conditions in fractured and non-fractured core samples, the impacts from a wide selection of parameters have been studied. It was found that the initial water saturation greatly impacts oil recovery from CO_2 injection. Higher S_{or} after waterflooding provided higher oil recovery from subsequent injection of CO_2 and

higher S_{wi} gave higher total oil recovery by waterflooding followed by CO_2 injection. Oil recovery from injection of CO_2 in the fractured, strongly water-wet core was significantly less (9.4 %OIP) than the non-fractured cores (17.0 %OIP and 40.6 %OIP) due to CO_2 escaping through the fracture network. Impacts from wettability on oil recovery during injection of CO_2 were not evident in this study with only six core samples.

The use of *in situ* saturation imaging techniques gained confidence of the obtained results, assisted in the investigation of recovery mechanisms, corroborating similar measurements using conventional methods and increased knowledge of multiphase fluid flow in porous rocks during a variety of production scenarios.

Future perspectives

During the experimental work in this thesis, the impacts from a wide range of reservoir and fluid properties on oil recovery have been studied using a selection of complimentary tools to measure *in situ* pressure and saturation during continuous flooding.

Paper 1 reports the experiments with simultaneous pressure and saturation measurements which provided data to obtain dynamic capillary pressure curves, to determine Amott-Harvey indices of wettability and to calculate relative permeabilities. Further discussions and experiments on Amott-Harvey indices of wettability and relative permeabilities are presented in ***Paper 2*** and ***Paper 3***, respectively. In order to improve the pressure measurements in future experiments, a different setup should be applied. Exchanging the pressure transducers connected to the core samples with five meters of plastic tubing with phase pressure membranes attached directly to the core samples would improve the accuracy and prevent any time delay in the pressure readings. Fluid saturation imaging using 3D CT would allow the use of phase pressure membranes, provide high spatial resolution measurements and improve the time resolution during continuous flooding. The results should also be supported by more numerical simulations.

The impacts from establishing capillary continuity between two isolated matrix blocks on the capillary end effect obtained by filling the separating fracture with micro-particles are reported in ***Paper 4***. The experimental data would benefit from applying MRI or CT to increase the spatial resolution in the fluid saturation measurements, improving the accuracy of the measurements and allowing recovery mechanisms in the fracture at different wettabilities to be monitored. During the experiments reported in this thesis, a chemical reaction between the oil phase and some of the micro-particles was observed, and an effort should be made to find different particles suitable for this purpose in future studies.

Paper 5 and ***Paper 6*** demonstrate the EOR potential from injection of liquid or supercritical CO_2 in fractured and non-fractured low-permeable chalk core samples at different wettabilities and initial saturations at secondary and tertiary conditions. The waterfloods and subsequent injections of CO_2 were monitored using MRI to study recovery mechanisms and determine oil recovery from isolated core pieces. In order to continue with the project the MRI intensity response to CO_2 when mixing with n-Decane needs to be determined, including measurements of relaxation times in addition to conventional spin-echo imaging. Future work on the project would include

1) studies of EOR from injection of CO_2 in oil-wet carbonates,

2) exchanging n-Decane with different types of crude oil to study more realistic scenarios and different recovery mechanisms,

3) the use of foam or gel in fractured core samples to reduce fracture permeability and thus divert the CO_2 into the matrix,

4) investigating CO_2 flow and storage potential in porous media using MRI.

Bibliography

Abdassah, D., Siregar, S. and Kristanto, D.: "The Potential of Carbon Dioxide Gas Injection Application in Improving Oil Recovery", SPE International Oil and Gas Conference and Exhibition, Beijing, China, 2000.

Amott, E.: "Observations Relating to the Wettability of Porous Rock." Petroleum Transactions, 216: p. 156-162, 1959.

Anderson, W. G.: "Wettability Literature Survey - Part 2: Wettability Measurement." Journal of Petroleum Technology, November: p. 1246-1262, 1986.

Anderson, W. G.: "Wettability Literature Survey - Part 4: Effects of Wettability on Capillary Pressure." Journal of Petroleum Technology, October: p. 1283-1300, 1987a.

Anderson, W. G.: "Wettability Literature Survey - Part 5: The Effects of Wettability on Relative Permeability." Journal of Petroleum Technology, November: p. 1453-1468, 1987b.

Aspenes, E., Ersland, G., Graue, A., Stevens, J., Baldwin, B. A.: "Wetting Phase Bridges Establish Capillary Continuity Across Open Fractures and Increase Oil Recovery in Mixed-Wet Fractured Chalk." Transport in Porous Media, 74(1): p. 35-47, 2008.

Ayirala, S. C., Xu, W. and Rao, D. N.: "Interfacial Behavior of Complex Hydrocarbon Fluids at Elevated Pressures and Temperatures", International Conference on MEMS, NANO and Smart Systems, Banff, Alberta, Canada, 2005.

Bloch, F.: "Nuclear Induction." Physical Review, 70: p. 460-474, 1946.

Calvo, A., Paterson, I., Chertcoff, R., Rosen, M. and Hulin, J. P.: "Dynamic Capillary Pressure Variations in Diphasic Flows through Glass Capillaries." Journal of Colloid and Interface Science, 14: p. 384-394, 1991.

Chakravarthy, D., Muralidaharan, V., Putra, E., Hidayati, D. T. and Schechter, D. S.: "Mitigating Oil Bypassed in Fractured Cores During CO2 Flooding Using WAG and Polymer Gel Injections", SPE/DOE Symposium on Improved Oil Recovery, Tulsa, OK., USA, 2006.

Chierici, G. L.: "Novel Relations for Drainage and Imbibition Relative Permeabilities." SPE Journal, June: p. 275-276, 1984.

Corey, A. T.: "The Interrelation between Gas and Oil Relative Permeabilities." Producers Monthly, 19: p. 38-41, 1954.

de Gennes, P. G.: "Dynamic Capillary Pressure in Porous Media." Europhysics Letters, 5: p. 689-691, 1988.

Dunn, K.-J., Bergman, D. J. and Latorraca, G. A.: "Nuclear Magnetic Resonance Petrophysical and Logging Applications", Helbig, K. and Treitel, S., 32, 2002.

Ekdale, A. A. and Bromley, R. G.: "Trace Fossils and Ichnofabric in the Kjølby Gaard Marl, Uppermost Cretaceous, Denmark." Bulletin of the Geological Society of Denmark, 31: p. 107-119, 1993.

Graue, A., Bognø, T., Moe, R. W., Baldwin, B. A., Spinler, E. A., Maloney, D. and Tobola, D. P.: "Impacts of Wettability on Capillary Pressure and Relative Permeability", International Symposium of the Society of Core Analysts, Golden, Co, USA, 1999.

Hassanizadeh, S. M., Celia, M. A. and Dahle, H. K.: "Dynamic Effect in the Capillary Pressure-Saturation Relationship and its Impacts." Vadose Zone Journal, 1: p. 38-57, 2002.

Heaviside, J., Black, C. J. J. and Berry, J. F.: "Fundamentals of Relative Permeability: Experimental and Theoretical Considerations", SPE Annual Technical Conference and Exhibition, San Francisco, California, USA, 1983.

Helmig, R., Weiss, A. and Wohlmuth, B. I.: "Dynamic Capillary Effects in Heterogeneous Porous Media." Computers & Geosciences, 11: p. 261-274, 2007.

Hild, G. P. and Wackowski, R. K.: "Reservoir Polymer Gel Treatments To Improve Miscible CO2 Flood." SPE Reservoir Evaluation and Engineering, 2(2): p. 196-204, 1999.

Holm, L. W.: "Miscibility and Miscible Displacement." Journal of Petroleum Technology, August: p. 817-818, 1986.

Honarpour, M. M., Huang, D. D. and al-Hussainy, R.: "Simultaneous Measurements of Relative Permeability, Capillary Pressure and Electrical Resistivity with Microwave System for Saturation Monitoring", SPE Annual Technical Conference and Exhibition, Dallas, Texas, USA, 1995.

Hughes, T. L., Friedman, F., Johnson, D., Hild, G. P., Wilson, A. and Davies, S. N.: "Large-Volume Foam-Gel Treatments to Improve Conformance of the Rangely CO2 Flood." SPE Reservoir Evaluation and Engineering, 2(1): p. 14-24, 1999.

Johnson, E. F., Bossler, D. P. and Naumann, V. O.: "Calculation of Relative Permeability from Displacement Experiments." Petroleum Transactions, 216: p. 370-372, 1959.

Kalaydjian, F.: "Effect of the Flow Rate on an Imbibtion Capillary Pressure Curve - Theory Versus Experiment", SCA European Core Analysis Symposium, Paris, France, 1992a.

Kalaydjian, F. J.-M.: "Dynamic Capillary Pressure Curve for Water-Oil Displacement in Porous Media - Theory vs Experiment", SPE Annual Technical Conference and Exhibition, Washington, DC, USA, 1992b.

Karaoguz, O. K., Topguder, N. N., Lane, R. H., Kalfa, U. and Celebioglu, D.: "Improved Sweep in Bati Raman Heavy-Oil CO2 Flood - Bullhead Flowing Gel Treatments Plug Natural Fractures." SPE Reservoir Evaluation and Engineering, April: p. 164-175, 2007.

Kolltveit, K., Nordtvedt, J. E., Hovland, F., Kvanvik, B. A. and Lie, B.: "Using Explicit and Implicit Methods to Calculate Relative Permeabilities from In Situ Measurements." Advances In Core Evaluation, I: p. 479-494, 1990.

Kulkarni, M. M. and Rao, D. N.: "Experimental Investigation of Various Methods of Tertiary Gas Injection", SPE Annual Technical Conference and Exhibition, Houston, Texas, USA, 2004.

Kulkarni, M. M. and Rao, D. N.: "Experimental investigation of miscible and immiscible Water-Alternating-Gas (WAG) process performance." Journal of Petroleum Science and Engineering, 48: p. 1-20, 2005a.

Kulkarni, M. M. and Rao, D. N.: "Experimental Investigation of Miscible Secondary Gas Injection", SPE Annual Technical Conference and Exhibition, Dallas, Texas, USA, 2005b.

Lackner, A. S. and Torsæter, O.: "Phase Pressure Measurements: Simultaneous and Direct Derivation of Relative Permeability and Dynamic Capillary Pressure", International Symposium of the Society of Core Analysts, Toronto, Canada, 2005.

Li, D. and Slattery, J. C.: "Analysis of the Moving Common Line and Dynamic Contact Angle formed by a Draining Film." Journal of Colloid and Interface Science, 143: p. 382-396, 1991.

Lomeland, F., Ebeltoft, E. and Thomas, W. H.: "A New Versatile Relative Permeability Correlation", International Symposium of the Society of Core Analysts, Toronto, Canada, 2005.

Mangalsingh, D. and Jagai, T.: "A Laboratory Investigation of the Carbon Dioxide Immiscible Process", Latin American and Caribbean Petroleum Engineering Conference and Exhibition, Port-of-Spain, Trinidad and Tobago, 1996.

Nagarajan, N. and Robinson Jr, R. L.: "Equilibrium phase compositions, phase densities, and interfacial tensions for carbon dioxide + hydrocarbon systems. 2. Carbon dioxide + n-decane.", Journal of Chemical and Engineering Data, 31(2): p. 168-171, 1986.

Ngan, C. G. and Dussan, E. B.: "On the Nature of the Dynamic Contact Angle: An Experimental Study." Journal of Fluid Mechanics, 118: p. 27-40, 1982.

Purcell, E. M., Torrey, H. C. and Pound, R. V.: "Resonance Absorption by Nuclear Magnetic Moments in a Solid." Physical Review, 69: p. 37-38, 1946.

Reference Fluid Thermodynamic and Transport Properties 8.0 (REFPROP), U.S. Secretary of Commerce, 2007

Schembre, J. M. and Kovscek, A. R.: "Direct Measurement of Dynamic Relative Permeability from CT Monitored Spontaneous Imbibition Experiments", SPE Annual Technical Conference and Exhibition, New Orleans, Louisiana, USA, 2001.

Sharma, M. M. and Wunderlich, R. W.: "The Alteration of Rock Properties Due to Interactions With Drilling Fluid Components", SPE Annual Technical Conference and Exhibition, Las Vegas, NV, USA, 1985.

Shyeh-Yung, J.-G. J.: "Mechanisms of Miscible Oil Recovery: Effects of Pressure on Miscible and Near-Miscible Displacements of Oil by Carbon Dioxide", SPE Annual Technical Conference and Exhibition, Dallas, Texas, USA, 1991.

Sigmund, P. M. and McCaffery, F. G.: "An Improved Unsteady-State Procedure for Determining the Relative Permeability Characteristics of Heterogeneous Porous Media." SPE Journal, February: p. 15-28, 1979.

Sydansk, R. D. and Southwell, G. P.: "More Than 12 Years of Experience with a Successful Conformance-Control Polymer Gel Technology", SPE Western Regional Meeting, Long Beach, California, USA, 2000.